Cryptococcus neoformans resist to drastic conditions by switching to viable but non-culturable cell phenotype

Benjamin Hommel[1,2,3*], Aude Sturny-Leclère[1*], Stevenn Volant[4], Nathanael Veluppillai[1], Magalie Duchateau[5], Chen-Hsin Yu[6], Véronique Hourdel[5], Hugo Varet[4,7], Mariette Matondo[5], John R Perfect[6], Arturo Casadevall[8], Françoise Dromer[1] & Alexandre Alanio[1,2,3,8]

[*] These authors participated equally to this work.

[1] Institut Pasteur, Molecular Mycology Unit, CNRS UMR2000, Paris, France

[2] Laboratoire de Parasitologie-Mycologie, Hôpital Saint-Louis, Groupe Hospitalier Lariboisière, Saint-Louis, Fernand Widal, Assistance Publique-Hôpitaux de Paris (AP-HP), Paris, France

[3] Université Paris Diderot, Sorbonne Paris Cité, Université de Paris, Paris, France

[4] Institut Pasteur - Bioinformatics and Biostatistics Hub - C3BI, USR 3756 IP CNRS, Paris, France

[5] Institut Pasteur, Unité de spectrométrie de masse et Protéomique, Paris, France.

[6] Division of Infectious Diseases, Department of Medicine, Duke University Medical Center, Durham, North Carolina, United States of America

[7] Institut Pasteur - Transcriptome and Epigenome Platform - Biomics Pole - C2RT, Paris, France

[8] Department of Molecular Microbiology and Immunology, Johns Hopkins Bloomberg School of Public Health, Baltimore, MD, USA

24 ***Corresponding Author:** Dr Alexandre Alanio, Molecular Mycology unit, Institut Pasteur, 25
25 rue du Dr Roux 75724 Paris Cedex 15; email: alexandre.alanio@pasteur.fr; Tel:
26 +33140613255; Fax: +33145688420

27 **Keywords**

28 *Cryptococcus neoformans*, viable but non culturable, reactivation, dormancy, growth,
29 latency, starvation, hypoxia, secretome, proteome, transcriptome, pantothenic acid, quorum
30 sensing

31 **Abstract**

32 Metabolically quiescent pathogens can persist in a viable non-replicating state for months or even
33 years. For certain infectious diseases, such as tuberculosis, cryptococcosis, histoplasmosis, latent
34 infection is a corollary of this dormant state, which has the risk for reactivation and clinical disease.
35 During murine cryptococcosis and macrophage uptake, stress and host immunity induce *C.*
36 *neoformans* heterogeneity with the generation of a sub-population of yeasts that manifests a
37 phenotype compatible with dormancy (low stress response, latency of growth). In this
38 subpopulation, mitochondrial transcriptional activity is regulated and this phenotype has been
39 considered as a hallmark of quiescence in stem cells. Based on these findings, we worked to
40 reproduce this phenotype in vitro and then standardize the experimental conditions to consistently
41 generate this dormancy in *Cryptococcus neoformans*.

42 We found that incubation of stationary phase yeasts (STAT) in nutriment limited conditions and
43 hypoxia for 8 days (8D-HYPOx) was able to produced cells that mimic the phenotype obtained in vivo.
44 In these conditions, mortality and/or apoptosis occurred in less than 5% of the yeasts compared to
45 30-40% of apoptotic or dead yeasts upon incubation in normoxia (8D-NORMOx). Yeasts in 8D-HYPOx
46 harbored a lower stress response, delayed growth and less that 1% of culturability on agar plates,
47 suggesting that these yeasts are viable but non culturable cells (VBNC). These VBNC were able to
48 reactivate in the presence of pantothenic acid, a vitamin that is known to be involved in quorum
49 sensing and a precursor of acetyl-CoA. Global metabolism of 8D-HYPOx cells showed some specific
50 requirements and was globally shut down compared to 8D-NORMOx and STAT conditions.
51 Mitochondrial analyses showed that the mitochondrial masse increased with mitochondria mostly
52 depolarized in 8D-HYPOx compared to 8D-NORMox, with increased expression of mitochondrial
53 genes. Proteomic and transcriptomic analyses of 8D-HYPOx revealed that the number of secreted
54 proteins and transcripts detected also decreased compared to 8D-NORMOx and STAT, and the
55 proteome, secretome and transcriptome harbored specific profiles that are engaged as soon as four

56 days of incubation. Importantly, acetyl-CoA and the fatty acid pathway involving mitochondria are
57 required for the generation and viability maintenance of VBNC.
58 All together, these data show that we were able to generate for the first time VBNC phenotype in
59 *Cryptococcocus neoformans*. This VBNC state is associated with a specific metabolism that should be
60 further studied to understand dormancy/quiescence in this yeast.
61

62 **Introduction**

63 All microorganisms are exposed to fluctuating environments and periodic external stresses,
64 which inhibit their growth. Some microbes may overcome these stress periods by entering
65 into a resistant non-replicative state, assessed by /associated with a decreased culturability
66 (1). This decrease was first assumed to reflect microbial death as a consequence of a
67 stochastic and induced nutrient deprivation decay (2). In quantum mechanics, the
68 Schrödinger's experiment considered a cat simultaneously alive and dead until a
69 measurement was made. A parallel experiment could be done with a dormant
70 microorganism. Answering if it is alive or dead seems trivial but is unquestionably uneasy (3).
71 In fact, there are two other alternative explanations. Non-culturable cells could be the
72 resulting state of a genetically programmed death or could be viable but non culturable cells
73 (VBNC) that are adapted to living / surviving but dormant cells like spores (4, 5). There is now
74 clear evidence that VBNC are viable cells with an intact cell membrane and a low metabolic
75 activity (6). Various environmental stressors can induce VBNC, such as starvation, hypoxia,
76 stressful temperature, pH variations (7). In a finalistic approach, to enable perpetuation of
77 the lineage, VBNC should be capable at some point to exit the dormant state to resume an
78 active and replicating form when environmental conditions improve. This process could be
79 described as reactivation or "resuscitation". At least 85 species of bacteria (8) and 10 species
80 of fungi (9–11) have been reported capable of adapting a VBNC state. Hence, the VBNC state
81 seems to be an intrinsic capability of many microorganisms including pathogenic ones (12–
82 15). During infection, the "dormant" pathogens are able to tolerate both immune system
83 attacks and prolonged exposure to antimicrobials (16). Pathogens are not known to cause
84 disease when present in the VBNC state but virulence is retained and infection can be
85 initiated again following reactivation (6).

86 Dormancy is an important pathogenic feature for some invasive fungal diseases, such as
87 cryptococcosis (17–19) and histoplasmosis (12), where dormant organisms are known to
88 reactivate years after primary infection. Cryptococcosis is caused by the ubiquitous
89 environmental basidiomycete yeast *Cryptococcus neoformans*. It occurs mainly in
90 immunocompromised individuals, and especially those with AIDS, with more than 200 000
91 new cases of meningoencephalitis and more than 180, 000 deaths per year worldwide (20).
92 Latency is an important phase of cryptococcosis pathogenesis. However, the "primary
93 complex" of infections has been rarely interrogated in contrast to tuberculosis (21).
94 Inhalation of infectious propagules leads to a primary pulmonary infection with a
95 granulomatous immune response (22) that either restrains infection or eradicates the yeast.
96 This immune response can fail when immunosuppression occurs leading to infection
97 reactivation and disease. Recently, evidence was reported for the existence of dormant
98 yeast cells of *C. neoformans* in models of *C. neoformans*/host interaction *in vivo* (mice) and
99 *in vitro* (macrophages) have been obtained (23). A population of dormant yeast cells
100 harboring characteristics that could be related to dormancy (low metabolic response,
101 growth latency, increased mitochondrial activity, increased autophagy, decreased
102 neoglucogenesis and reactivation by fetal calf serum) was described (23). To characterize
103 these cells, we needed reproducible *in vitro* conditions that would generate yeast cells with
104 a phenotype identical to that observed in the subpopulations of yeasts upon interaction with
105 hosts. Based on previous studies performed in skeletal muscle stem cells (24), we developed
106 an *in vitro* model using two consecutives stresses, i.e. nutrient starvation and hypoxia, and
107 used them to analyze the parameters influencing dormancy and reactivation of dormant
108 yeasts. Using phenotypic microarrays along with, proteome, secretome, and transcriptome
109 analyses, we further validated and characterized these yeast cells and their metabolic

110 pathways that are crucial for the generation, maintenance of and exit from this dormancy

111 state.

112 **Results**

113

114 **Yeasts incubated in hypoxia were intact and had low metabolic activity and delayed**
115 **growth**

116 Based on our previous identification of dormant cells in a mouse model of cryptococcosis
117 (23), we identified *in vitro* conditions that induced a phenotype in *C. neoformans* cells that
118 mimicked the phenotype observed *in vivo*. After defined pre-culture conditions, yeasts in
119 YPD liquid medium (stationary phase, STAT) were incubated in nutrient deprivation, hypoxia
120 (O_2<0.1%) and increased CO_2 concentration) at 30°C for 8 days (all subsequent will be
121 referred as 8D-HYPOx) (Supplementary Figure 1). Yeasts in hypoxia were then compared to
122 yeasts cultured in parallel in normoxia (referred as 8D-NORMOx), and to STAT.

123 Median body cell sizes were not different for yeasts in 8D-HYPOx, 8D-NORMOx compared to
124 STAT (4.5 µm; interquartile range (IQR) [3.8-5.1], 4.6 µm [4.1-5.0] and 4.6 µm [4.1-5.0],
125 respectively). Median capsule size was smaller in 8D-HYPOx (0.8 µm [IQR=0.7-1.0] and 8D-
126 NORMOx (0.9 µm [0.7-1.0]) compared to STAT, (1.0 µm [0.9-1.2]), (Supplementary Figure 2A
127 and B, p<0.0001). Specific staining revealed no differences in the shape of the nucleus
128 (Figure 1A), nor on the structure of the capsule based on E1 binding (Figure 1A,
129 Supplementary Figure 3A) but did show an increased quantity of vacuolar membrane (3.1 ±
130 0.4 increase in the geometric mean fluorescence 8D-HYPOx/8D-NORMOx cells compared to
131 STAT (Figure 1A, Supplementary Figure 3B). Plasma membrane was intact for the majority
132 (88%) of the cells in 8D-HYPOx, and for 60% of them in 8D-NORMOx compared to 98% in
133 STAT (Figure 1A, Supplementary Figure 3C). Transmission electron microscopy (TEM)
134 revealed a significantly thicker cell wall in 8D-HYPOx cells compared to STAT (median 206 nm

135 [170.5-245.0] and 163.5 nm [123.8-199.3], $p<0.05$, Supplementary Figure 2C) and the
136 presence of large intracytoplasmic vacuoles (Figure 1B).
137 Intracellular levels of glutathione as a marker of stress response in *C. neoformans* (23) was
138 assessed kinetically by CMFDA staining at day 0 (STAT) and 4, 6 and 8 d (D4, D6, D8). A
139 decrease in stress response was observed over time with an apparently homogenous
140 population harboring a low CMFDA intensity in 8D-HYPOx, as opposed to 8D-NORMOx
141 condition where a double population (low and high CMFDA intensity corresponding to low
142 and high stress response) was observed at D8 (Figure 1C). Growth curves in rich medium
143 (YPD) were determined at the same time points using mathematical modeling, with latency
144 (lag phase λ) as the major readout (Figure 1D). Median latency was significantly increased for
145 8D-NORMOx and 8D-HYPOx populations compared to STAT (1103 m [1083-1104] with a
146 continuous increase over time for yeast cells grown in 8D-HYPOx from 1387 m [1281-1445]
147 at D4, to 1878 m [1800-1898] at D8 whereas it plateaued in 8D-NORMOx (1194 m [1176-
148 1210] at D4, and 1288 m [960-1351] at 8D (Figure 1E).
149

150 **Yeasts incubated in hypoxia were mostly viable but non-culturable cells (VBNC)**

151 Cell viability and yeast apoptosis-like phenomenon measured over time evolved differently
152 in hypoxia and normoxia (Figure 2A). Viable non-apoptotic cells represented 98.7% [98.4-
153 99.0]) in the STAT condition, and almost the same proportion (98.9% [98.8-99.0]) at 8D-
154 HYPOx with a decrease at D2 D4 and D6, culminating at 74.6% [70.5-78.8] at D4. In
155 normoxia, that proportion decreased and plateaued at D8 at 63.6% [62.2-65.0]. The
156 proportion of apoptotic-like cells, negligible in STAT cells (0.8% [0.5-1.6]), peaked at D4 in
157 hypoxia (21.4% [17.5-25.4]) while it increased over time to reach a plateau at D6 in normoxia

158 (35.8% [34.9-36.7]). Dead cells represented less than 3% over time in hypoxia (2.7% [1.7-3.7]
159 at D4), while it reached 5% [4.2-5.9] at D6 in normoxia and was less than 1 % in STAT.
160 Culturability (proportion of culturable yeasts) assessed over time by colony forming unit
161 (CFU) on YPD agar was decreased in both conditions but significantly more in 8D-HYPOx than
162 in 8D-NORMOx (17.5% [15.4-19.7], vs. 0.8% [0.5-1.0] $p<0.01$) (Figure 2B)
163 The population of cells observed at 8D-HYPOx was heterogeneous in terms of CMFDA
164 staining, a small quantity harbored a high CMFDA staining (high stress response). We thus
165 hypothesized that they were the metabolically active cells responsible for the observed
166 growth. Consequently, yeast populations were sorted according to their CMFDA intensity
167 (low, medium and high). The latency of the three populations was comparable to that of the
168 unsorted (bulk) population and significantly higher than in the 8D-NORMOx and STAT
169 conditions (Figure 2C). Likewise, culturability assessed by plating the cells suspension on
170 Sabouraud agar plates was not significantly different in $CMFDA^{low}$ (0.19±0.20), $CMFDA^{medium}$
171 (0.28±0.17), $CMFDA^{high}$ (0.10±0.11) compared to the unsorted population (0.53±0.41)
172 ($p>0.01$), although significantly lower than in 8D-NORMOx (12.73% [7.62-18.62]) and STAT
173 (102.5% [93.25-111.8]) conditions (Figure 2C, $p<0.01$). Culturability assessed by counting the
174 proportion of culture-positive wells after 5 d of incubation for 3333 cells per well showed
175 also a decrease in culturability with 10 positive wells/18 seeded (55.5%) for the $CMFDA^{low}$,
176 16/18 (88.8%) for the $CMFDA^{medium}$, 14/18 (77.7%) for the $CMFDA^{high}$, and 17/18 (94.4%) for
177 the unsorted populations whereas all wells (100%) grew in the 8D-NORMOx (6/6) and STAT
178 (3/3) conditions.
179 These results suggested that the combination of hypoxia and nutrient depletion led to the
180 production of a population mostly composed of what is called viable and non-culturable cells

181 (VBNC). A model for the evolution of the cell population phenotypes over time in hypoxia
182 and normoxia is proposed in Figure 2D.
183
184 **Factors influencing latency**
185 Latency of growth can be influenced by numerous factors. We first tested cell concentration
186 and culture medium. Serial 10-fold dilutions of the cells ($3x10^5$ to 3/well) resulted in an
187 increased latency for both 8D-HYPOx and STAT cells, in YPD and in minimal medium (MM)
188 (Supplementary Figure 4A-B). The latency was higher in MM than in YPD for 8D-HYPOx at all
189 the dilutions studied (Table 1) and for STAT at all dilutions except for $3x10^3$/well. Nonlinear
190 fitting permitted the extrapolation of the best fit curve and showed that a low nutrient
191 medium (MM) increased the latency by a differential of 2505 m for STAT and 2656 m for 8D-
192 HYPOx compared to a richer medium (YPD). There was almost no difference in latency for 1
193 cell between STAT and 8D-HYPOx: for 1 cell the latency (8D-HYPOx -STAT) was 1820 m for
194 YPD and 1971 m for MM.
195
196 **8D-HYPOx can be reactivated by pantothenic acid (PA), the acetyl CoA precursor.**
197 We hypothesized that the latency observed for the 8D-HYPOx population could be impacted
198 by the quantity of nutrients available in the medium, a parameter that could be simulated by
199 dilution of MM in water. MM dilutions resulted in a significant decrease in 8D-HYPOx latency
200 from 4463 m [3947-5488] in 100%MM to 3722 m [3612-4156] in 20%MM and 3358 m [3240-
201 3664] in 10%MM ($p<0.01$, Figure 3A). This decrease was also observed for STAT but to a
202 lesser extent (1593 m [1397-1720], 1326 m [1220-1510] and 1245 m [1045-1277] in
203 100%MM 20%MM and 10%MM, respectively, $p <0.01$).

204 One of the major characteristics of viable but not culturable cells (VBNC) is that they can be
205 reactivated under various conditions which should translate into decrease of latency. Thus,
206 we tested the effect on 8D-HYPOx of conditioned medium (freeze-dried and rehydrated MM
207 from STAT populations), murine macrophage cell lysates (J774 cell line), pantothenic acid
208 (PA, vitamin B5), thiamine (vitamin B1), sodium pyruvate, and L-DOPA. Latency decreased
209 only upon addition of J774 lysate, conditioned medium and PA. As conditioned medium and
210 J774 lysate are each complex media rich in PA, we decided to focus specifically on the effect
211 of PA, which was previously implicated in quorum sensing effects (25). Addition of PA to
212 100%MM showed a dramatic effect on the latency of 8D-HYPOx. For instance, latency was
213 decreased at concentrations of PA above 1.25 x 10^{-2} µM from 3994 m [3797-4332] (no PA)
214 and 4111 m [3866-4451] (1.25 x 10^{-4} µM) to 2213 m [1963-2426] for (1.25 x 10^{-2} µM), 2095 m
215 [2007-2170] (1.25 µM) and 2133 m [2035-2281] (125 µM), respectively (Figure 3B, $p < 0.01$).
216 In comparison, less effect of PA was observed on STAT cells (from 1615 m [1532-1637] (no
217 PA) to 1433 m [1398-1456] (1.25 x 10^{-4}µM) and then 1036 m [1017-1045] (1.25 x 10^{-2}µM),
218 1048 m [1017-1045] (1.25 µM), 1018 m [982.5-1031] (125 µM)).
219 We compared the growth curves to investigate if a change in growth rate was induced by PA
220 or diluted MM. An increased slope would correspond to an increased growth rate, meaning
221 an increased speed of cell generation during exponential phase. MM dilutions (20%MM and
222 10%MM) significantly decreased growth rate of hypoxia cells compared to 100%MM but did
223 not alter STAT cells (Figure 3C). PA significantly increased growth rate of 8D-HYPOx at
224 concentrations above 1.25 µM and of STAT cells at concentrations above 1.25 x 10^{-2}µM
225 (Figure 3D, $p < 0.01$).
226 To understand whether the reactivation observed was due to an increased number of
227 growing cells or to an improved metabolic adaptation in 8D-HYPOx, limit dilutions

228 experiments were performed calculating the probability for one cell to grow (Supplementary
229 Figure 4C). Dilution of MM alone (10%MM) did not modify the median proportion of
230 culturable cells. Addition of PA increased significantly the median proportion of culturable
231 cells from 1.3 ‰ [0.8-1.9] to 2.5 ‰ [2.0-3.3] in 100%MM and from 1.1 ‰ [0.9-1, 4] to 2.5 ‰
232 [2.1-2.7] in 10%MM. ($p < 0.01$, Figure 3E). Culturability of yeasts did not change upon
233 interaction with macrophages with a comparable median proportion of culturable yeast cells
234 in 8D-HYPOx before (1.04 ‰ [0.78-1.48]) and after 2 h macrophage uptake (1.21 ‰ [1.09-
235 1.33], $p=0.35$; Supplementary fFgure 4D).
236 Overall, when decreasing nutrient availability (diluting medium), latency decreased without
237 change in the number of culturable yeast cells, suggesting that culturable yeast cells were
238 better adapted to grow in poor than in richer medium. By contrast, addition of PA allowed
239 VBNC to switch to culturable cells (cell reactivation) with a decreased latency reflected an
240 increasing number of culturable cells. However, the 2-fold increase in culturability after
241 addition of PA was not sufficient to explain the extent of the decrease in latency suggesting
242 that PA influences also growth adaptation (Figure 3F). From now on, 8D-HYPOx yeast cells
243 are called VBNC for convenience.
244
245 **VBNC showed specific metabolic requirements and general low metabolic activity**
246
247 To explore the VBNC phenotype further, their metabolic profile was obtained using Biolog®
248 substrate utilization tests and compared with that of yeast cells in other conditions. Based
249 on the 761 metabolites tested and excluding 240 compounds positive in the dead cells
250 control, hierarchical clustering showed that VBNC possessed a unique profile (Figure 4A).
251 VBNC had significant lower global metabolic activity (median= 124.0 [94.0-173] and 87.0

252 [65.0-118.8]) compared yeast cells in 8D-NORMOx (246.0 [106.8-260.0] and 248.5 [123.0-
253 262.0] for the two biological replicates) and to STAT (262.0 [136.5-272.0]) ($p<0.01$, Figure
254 4B). Finally, we identified two compounds (trimetaphosphate; Adenosine-2', 3' cyclic
255 monophosphate) that were more metabolized by VBNC than by control yeast cells
256 (Supplementary Table 1).
257

258 **VBNC have increased mitochondrial mass and depolarized mitochondria**

259 Since the phenotypic microarrays based on mitochondrial activity measurement showed a
260 decrease in VBNC (8D-HYPOx), we tested further various mitochondrial parameters. ROS and
261 RNS production were slightly decreased in VBNC compared to STAT cells with median 152.3
262 [148.1-156.2] vs. 174.1 [168.9-177.8] using the ROS probe ($p<0.01$) and 87.1 [78.2-101.2] vs.
263 149.5 [98.7-206.5] using the RNS probe, respectively ($p<0.01$) (Supplementary Figure 5).
264 Using multispectral flow cytometry, we observed an increase in the mitochondrial mass in
265 VBNC and in 8D-NORMOx cells compared to STAT and dead yeast cells using Mitotracker
266 staining. JC-1 and TMRE staining revealed that the mitochondria in VBNC are mostly
267 depolarized (low TMRE and high JC-1 fluorescence) (Figure 5A-B). The expression of the
268 mitochondrial genes CYTb, NADH, mtLSU and COX1 significantly increased in 8D-HYPOx
269 compared to STAT ($p=0.029$) (Figure 5C), and DNA quantification remained similar ($p<0.05$).
270

271 **VBNC have a reduced but a specific secretome and a specific proteome**

272 Secreted protein in the supernatant (secretome) and cellular proteins (proteome) were
273 analyzed in STAT, VBNC (8D-HYPOx) and 8D-NORMOx using both qualitative and quantitative
274 analysis of the proteins recovered in triplicate.

275 In VBNC, a total of 1365 proteins were identified within the secretome and 3772 proteins
276 within the proteome. In the secretome, the median number of secreted proteins identified
277 (starting from 747 proteins [598-797] in STAT) decreased up to (411 [406-460]) in VBNC
278 compared to 8D-NORMOx (910 [909-928]) (Supplementary Figure 6A, $p < 0.001$). The protein
279 concentrations in the secretome remained stable in VBNC and slightly increased in 8D-
280 NORMOx yeast cells (Supplementary Figure 6B, Supplementary Table 2). In the proteome,
281 the median number of proteins identified (starting from 2975 proteins [2951-3029] for STAT)
282 was stable over time in hypoxia and normoxia (3057 [3033-3171] in VBNC and 2968 [2960-
283 2976] in 8D-NORMOx Supplementary Figure 6C). The protein concentration in the proteome
284 (0.005 mg/mL [0.002-0.011] in STAT) tended to increase for both yeast cells reaching 0.017
285 mg/mL [0.008-0.018] for VBNC and 0.021 mg/mL [0.016—0.027] for control yeast cells)
286 (Supplementary Figure 6D).
287 We then analyzed the proteins that differed between STAT and VBNC/8D-NORMOx in the
288 secretome and the proteome. Overall, 17/ 1365 proteins present in the secretome, and
289 107/3772 present in the proteome were specifically found only in VBNC cells
290 (Supplementary Figure 7A-7B and Supplementary Table 3).
291 When secreted proteins and cellular proteins were pooled, the analysis found 226 proteins
292 present in all six conditions (Figure 6A). A total of 1654 proteins were found exclusively in
293 the proteome common to the 3 conditions, or exclusively in STAT (n=150), in control (n=75)
294 or in VBNC (n=103) (Figure 6A). A total of 17 proteins were detected exclusively in the
295 secretome common to the 3 conditions with 6 exclusively in STAT and hypoxia (but
296 different), and 16 exclusively in normoxia (Figure 6A, Supplementary Table 4).
297 For the subsequent analysis, the whole kinetics in hypoxia and normoxia was analyzed
298 (STAT, hypoxia and normoxia (D4, D6 and D8)). GO enrichment analysis of the proteins

299 present in in the secretome showed differences in the biological processes, molecular
300 functions and molecular components, whereas similar patterns and distributions were
301 observed for the proteome. Thus, in the secretome of hypoxia (D4, D6 and VBNC: D8) the
302 major enriched biological processes were translation and metabolic processing of
303 carbohydrates and in Normoxia (D4, D6 and D8), the major enriched biological processes
304 were related to oxidation-reduction mechanisms with no major change over time (Figure
305 6B). The enriched molecular functions and components were also different (supplementary
306 Figure 8A and B and Supplementary Table 5). For instance, in the proteome, in both hypoxia
307 and normoxia kinetic, the translation, oxidation-reduction biological processes (Figure 6C),
308 the nucleotide binding transferase activity and the catalytic activity for molecular functions
309 and the cytoplasm, ribosome, ribonucleoprotein and intracellular components were
310 significantly enriched (Supplementary Figure 8C and D and Supplementary Table 5).
311 Principal coordinate analysis (PCA) analysis of the global data revealed that the distance
312 between conditions for the secretome (Figure 7A) and the proteome (Figure 7C evolved
313 from STAT differently in hypoxia and normoxia conditions. An independent and specific
314 pattern was seen as soon as day 4 in hypoxia and normoxia. We then selected the proteins
315 present in all conditions and analyzed how the level of each protein evolved over time.
316 Overall, 85 secreted proteins were differentially produced, including 49 under normoxia and
317 36 in hypoxia (Supplementary Table 6) and 63 cellular proteins were differentially produced
318 including 47 significantly more produced in normoxia and 16 in hypoxia (Supplementary
319 Table 6). Based on these results, hierarchical clustering of the secretome (Figure 7B) and the
320 proteome (Figure 7D) was performed. It demonstrated that STAT specimens clustered
321 together with the normoxia specimens for the secretome, whereas they clustered with
322 hypoxia specimens for the proteome.

323 Among the 16 cellular proteins overproduced during hypoxia, one was a serine
324 carboxypeptidase (CNAG_06640); one is associated with intracellular transport
325 (CNAG_07846); 6 were associated with the processing of DNA / RNA and the cell-cycle
326 (CNAG_01455, CNAG_04570, CNAG_00819, CNAG_06079, CNAG_05311 and CNAG_04962),
327 and the 9th protein is linked to the mTOR pathway (CNAG_01148, also known as FK506-
328 binding protein) (Table 2). The other 7 proteins have no known roles (hypothetical proteins).
329 Cellular proteins overproduced in normoxia were subsequently, down produced in hypoxia.
330 These 47 proteins down produced in hypoxia were mostly proteins from the fatty acid
331 degradation pathway, the glyoxylate cycle: isocitrate lyase (CNAG_05303), malate synthase
332 (CNAG_05653) and a protein of the neoglucogenesis, the phophoenolpyruvate
333 carboxykinase (CNAG_04217).
334
335 **Fatty acid pathway is required in VBNC**
336 STRING analysis was used to visualize the predicted protein-protein interactions for the 63
337 cellular proteins differentially produced by VBNC (Figure 8A). Several metabolic pathways
338 were identified, but especially the fatty acids metabolic pathways: degradation and
339 metabolism of fatty acids, degradation of α-ketoacids (valine, leucine and iso-leucine),
340 metabolism of alpha-linolenic acid, beta-alanine and elongation of fatty acids as well as
341 peroxisomes. To examine whether VBNC stored fatty acids better than STAT or 8D-Normox,
342 Bodipy®. 505/515 that stains neutral lipids in lipids droplets was used but no difference was
343 observed (Figure 8B). The β oxidation pathway described in the KEGG database was used to
344 visualize the 63 cellular proteins differentially produced in VBNC and the 8 proteins for fatty
345 acid degradation metabolism (Figure 8C). The fatty acid degradation pathway (β oxidation) is
346 well-characterized in *Saccharomyces cerevisiae* with several genes found also in *C.*

347 *neoformans* genome (Figure 8D). Interestingly, the corresponding proteins in *C. neoformans*
348 were known to be under produced in VBNC. The 9 deletion mutants of proteins identified
349 from the KEGG database and by the orthology with *Saccharomyces* genome available in the
350 Madhani collection were tested in the model for their ability to generate VBNC. A significant
351 decreased in the proportion of living cell was measured for 04688Δ, 00490Δ, 07747Δ and
352 00524Δ, all directly involved in fatty acid degradation (Figure 8E, $p<0.01$), suggesting that the
353 fatty acid pathway is required in VBNC although the level of expression is lower than in STAT
354 cells.
355

356 **VBNC cells have reduced but specific transcriptome**

357 We then compared genes expression in the three conditions using transcriptome analysis. To
358 avoid bias related to decreased RNA content and not in gene expression, we performed a
359 specific experiment in which we spiked each sample with the same quantity of *S. cerevisiae*
360 prior to extraction allowing us to normalize the transcription of *C. neoformans* to that of *S.*
361 *cerevisiae*. The number of transcript was decreased in VBNC, and to a lesser extent in 8D-
362 NORMOx, compared to STAT and LOG conditions that harbored similar level of transcripts
363 (Figure 9A).
364 PCA analysis of the global transcriptomic data from non-spiked samples suggested an
365 evolution from LOG to STAT phases with a clear independent and specific route leading to
366 VBNC or control yeast cells (Figure 9B). GO enrichment analysis of upregulated transcripts
367 showed that the major biological processes involved were: signal transduction, ATP synthesis
368 coupled proton transport and regulation of ARF protein signal transduction in VBNC,
369 oxidation-reduction, protein folding and response to stress in control and oxidation-
370 reduction and translation in LOG (Figure 9C). Further analysis revealed the clustering into 7

371 clusters that clearly separate the transcriptional profile of the 4 experimental conditions
372 (LOG, STAT, VBNC, 8d-NORMOx, Figure 9D). Specifically, cluster 4 appeared to be composed
373 of genes upregulated in hypoxia compared to the other conditions which underlying
374 pathways are summarized in Table 3 and Supplementary Table 7.

375 **Discussion**

376 We report the existence of a *C. neoformans* phenotype whereby dormant cells *in vitro* are
377 viable but not culturable cells (VNBC). Hence, *C. neoformans* joins the ranks of microbes
378 where similar phenomena have been described (6, 8, 10, 12–16) with the proviso that for
379 this organism this phenotype has obvious clinical importance given that latency is a common
380 manifestation of human infection.

381 Latency of cryptococcosis that can be linked with dormancy of *C. neoformans* had been
382 characterized clinically (26, 27) and epidemiologically (17, 18). This population of dormant
383 yeasts is thought to be located in a pulmonary granuloma but other reservoirs could exist
384 (23, 28). Recently, evidence for the existence of dormancy in a sub population of *C.*
385 *neoformans* upon interaction with the host *in vivo* (murine infection) and with macrophages
386 *in vitro* (23). To obtain homogenous population of dormant an *in vitro* protocol was set up
387 here using stresses known to generate quiescence: nutrient starvation after a first culture in
388 rich liquid culture medium and hypoxia (29–31). After eight days in hypoxia, the cells (8D-
389 HYPOx) were alive with a preserved structure but with more vacuoles than stationary phase
390 (STAT) cells. Then, when assessed for an apoptosis-like phenotype (32), viability and
391 culturability, we concluded that 8D-HYPOx condition was able to generate a homogeneous
392 population of viable but non-culturable cells (VBNC) with <1% apoptotic, > 99% viable and
393 <0.01% cultural cells. This phenotype is associated with dormancy in other microbial
394 populations (6–8, 10, 33). In contrast, 8D-NORMOx yeast population were very
395 heterogeneous with an increased death rate and apoptosis and higher culturability. We
396 observed that hypoxia turned almost the entire *C. neoformans* population into VBNC
397 phenotype starting after 4 days of hypoxia suggesting that hypoxia was a protective factor
398 against apoptosis. Hypoxia is an important factor to induce dormancy of mammalian stem

399 cells (34). Hypoxia is also present to some extend in the granuloma (35–37). In stem cells,
400 hypoxia is required for a strict metabolic regulation to maintain long-term quiescence and
401 self-renewal of populations. Hypoxia is also known to influence cell fate (differentiation, de-
402 differentiation) within the stem cell niche (38, 39). In addition, resistance to apoptosis is
403 known in mammalian cells by the induction of apoptosis inhibitors such as IAP-2 (40, 41) but
404 opposite results have been found with tumor cells (42). Nevertheless, by using these in vitro
405 conditions to generate what happened to be VBNC, we acknowledge that the phenotype
406 obtained could be different from the sub-population of dormant yeasts identified from the
407 lung of infected mice in our lab (23), although similarities are observed (low stress response
408 through CMFDA decreased fluorescence, latency of growth, increased mitochondrial
409 transcription). One important additional point is that there is technical limitation to work
410 with dormant yeasts from murine infection because of the low number of yeasts present in
411 the lung (10^4 cells recovered from the sacrifice of 42 animals) and the necessity to sort them
412 and by doing so impact their phenotype (23).
413 In VBNC-inducing conditions, the yeast population experienced an increased latency (lag
414 phase) over time. We investigated by different means if this delay was due to the decreased
415 number of cells able to grow or the decreased metabolic activity capacity. We validated in *C.*
416 *neoformans* that the difference in latency depended on nutrient availability (difference
417 between poor (MM) and rich (YPD) media), and on the number of cells able to grow
418 (dilutions of STAT yeasts). In addition, we showed that the metabolic activity of the cells was
419 also an important factor that participated in latency.
420 One of the major characteristics of cells manifesting the VBNC phenotype is their ability to
421 be reactivated - to divide again - in response to specific stimuli (7, 43, 44). Indeed, the final
422 demonstration of the existence of the VBNC phenotype came with the identification of

423 conditions that allowed reactivation. Among them, YPD-conditioned media, murine
424 macrophage lysate and PA had the greatest impact on latency under our conditions. YPD
425 medium and murine macrophage lysate are in fact complex media that also contained PA
426 (45), so we focused on PA alone. We hypothesized that PA was an important factor in
427 reactivating VBNC based on the fact that PA was known to decrease latency in *C.*
428 *neoformans* cells (46) and was also a known beneficial secreted compound by *C. neoformans*
429 (25). By adding PA to culture medium it decreased latency of VBNC but had less effect on
430 STAT.
431 We observed that MM dilutions increased growth capacities of VBNC (decreased latency). To
432 explain this counterintuitive observation, we propose that exposure to a high amount of
433 nutrients after long-term starvation was deleterious for yeast cells that had to resume
434 normal metabolism, possibly as a result of oxidative damage as metabolism increases, and
435 this hypothesis is further based on the fact that death was shown by others to be
436 accelerated in rich substrate (47–49).
437 Given that the critical issue in an reactivation experiments is to distinguish between an
438 increased number of cells from reactivation of the VBNC state from faster growth of already
439 present culturable cells, a method was developed to measure the probability of growth for
440 one yeast cell, inspired by the most probable number method (50). We found that the effect
441 of PA and medium dilution was different on VBNC cells compared to STAT cells. The effect of
442 PA on VBNC was a result from the doubling number of reactivated VBNC and from an
443 increase in growth rate. The weight of each factor remains to be determined. The proportion
444 of VBNC that was reactivated was in fact low (1.2‰). It is highly probable that resuscitation
445 of VBNC may require other factors that still need to be discovered. In our system, the
446 majority of the yeast population was probably not able to reactivate as hypoxia may have

447 pushed the yeasts too far into the process of dormancy for them to be reactivated or
448 without resuscitation (51). Indeed, the VBNC population may be injured while still alive and
449 unable to divide again (52). On the other hand, the MM dilution did not influence VBNC
450 reactivation culturability but rather decreased the growth rate by a faster rewire of the
451 metabolic state of the remaining culturable cells.

452 Despite the importance of *Cryptococcus*-protozoan interaction in the explanation of its
453 virulence and intracellular pathogenic strategy (53), we showed that macrophage uptake of
454 VBNC had no effect on culturability. This result is different from what was observed for other
455 microorganisms. For example, reactivation of VBNC was possible for the bacterium *L.*
456 *monocytogenes* and the protozoans *Acanthamoeaba polyphaga* (54) and *A. castellanii* (55).

457 We first screened our dormancy phenotype through the decrease in metabolic and stress
458 responses (23), as measured upon staining with the CMFDA fluorescent probe (56, 57).
459 Although it allowed us to detect that hypoxia was an important factor for the generation of
460 VBNC, we observed surprisingly that the culturability of the yeasts was independent of the
461 CMFDA level after sorting the different CMFDA populations. This suggested that CMFDA
462 staining is not a perfect marker of metabolic and stress response in *C. neoformans*.

463 Decreased metabolic activity in VBNC was demonstrated by several strategies. First, a
464 phenotypic array measurement (Biolog®) allowed us to show a reduction in the metabolism
465 of 761 compounds in VBNC. Second, we also noticed that the concentration of secreted or
466 intracellular proteins was lower in VBNC compared to 8D-NORMOx as reported during
467 quiescence in other organisms (58–61). We observed that the number of secreted proteins
468 present in the supernatant of VBNC decreased over time compared to the 8D-NORMOx
469 control. In parallel, the increase in the number of proteins present in the supernatant of 8D-
470 NORMOx could correspond to increased secretion but more likely to an increased release of

471 proteins due to a high cellular mortality observed in that condition. Third, using a unique
472 strategy of analysis for the transcriptome including the spike of a definite % of Log phase *S.*
473 *cerevisiae* cells, we demonstrated a global decreased transcriptional activity in 8D-HYPOx
474 compared to 8D-NORMOx, LOG and STAT conditions, identifying again the lower metabolic
475 activity of VBNC.
476 In 8D-HYPOx, we found that the mitochondrial phenotype was modified compared to STAT
477 condition, an included increased mitochondrial mass (increased mitotracker and JC-1
478 fluorescence) depolarization (TMRE low and JC-1 high), assessed by imagestream X and an
479 increased expression of mitochondrial genes without an increase in the quantity of
480 mitochondrial DNA between 8D-HYPOx and STAT. This observation could explain why ROS
481 and RNS levels are lower in VBNC compared to STAT. This depolarized state could also reflect
482 activation of autophagy (62). These results are reminiscent of those obtained in the dormant
483 subpopulation of yeasts observed in mice 7 days after infection and in macrophages, where
484 *COX1* and autophagy genes (*ATG9* and *VPS13*) have been shown to be upregulated
485 compared to other subpopulations of yeasts (23).
486
487 We identified and quantified proteins from the secretome (supernatant) and proteome (cell
488 pellet) over time. A qualitative proteomic analysis of secreted and cellular proteins in the
489 three conditions: STAT, VBNC and 8D-NORMOx showed different protein profiles, which
490 allowed the identification of proteins specific for hypoxia including 7 secreted and 103
491 cellular proteins. Overall, 1365 secreted proteins were identified. This number is greater
492 than previously described (63–65) but the protein extraction methods differed (gel
493 extraction, TCA / acetone precipitation alone) and the identification procedures and the
494 culture media used (YPD or MM) were different. Nevertheless, of the 191 secreted proteins

495 previously identified in stationary phase in YPD (63–65), 93.7% were found in our
496 corresponding sample (STAT with 565 proteins identified in all of the 3 replicates). In *C.*
497 *neoformans*, the secreted molecules can take several pathways to reach the periphery of the
498 cell and the extracellular space. There are conventional and unconventional secretory
499 pathways involving secretory machinery in protein export: Sec4, Sec6, Sec14, the Golgi
500 apparatus, and extracellular exosome vesicles (66–68). Our analysis of the secreted proteins
501 within the supernatants, since the TCA precipitation step used will precipitate soluble
502 proteins and also those in extracellular vesicles (69). Consequently, we are unable to
503 precisely identify their mechanism of secretion. These studies will be performed in the but
504 this opens future directions for study to understand the relationship between dormancy and
505 extracellular vesicles. Interestingly, a secreted protein, pqp1 peptidase (CNAG_00150) was
506 found overexpressed in hypoxia. This peptidase cleaved the pro-qsp1 quorum sensing
507 peptide into qsp1 (CNAG_03012), that acts on the whole cell population and regulates
508 virulence (70–72). However, we did not find qsp1 in the supernatants of the culture media
509 and yet it is present in micromolar amounts in the publication of Homer et al. (70). It is
510 possible that our extraction protocol was not optimized for small peptides (11 amino acids)
511 or that small peptides might have been eliminated through the various washings steps. The
512 analysis of the total proteome under hypoxia conditions allowed the identification of 3772
513 cellular proteins which is more than previously reported in *C. neoformans* (64, 73–75) and is
514 likely due to the optimized extraction method. PCoA analyzes of the secretome and
515 proteome kinetics showed a specific profile in VBNC and normoxia conditions compared to
516 STAT. The hierarchical clustering of the secretome reinforced the finding that VBNC was the
517 more distant condition compared to normoxia conditions and STAT. However, proteome
518 hierarchical clustering showed that STAT and day 4 hypoxia were close to each other and

519 that normoxia proteome was clearly different. The GO enrichment analysis revealed specific
520 functions of the secreted proteins in hypoxia compared to normoxia, whereas the pattern
521 was similar in the proteome: biological processes involving translation, carbohydrate
522 metabolism and glycolysis were enriched in the secretion of hypoxia cells.
523 The quantitative proteome analysis revealed that 16 proteins were more produced in
524 hypoxia, including CNAG_01148 also known as FK506-binding protein which is involved in
525 the mTOR pathway, and has a role in quiescence in *S. cerevisiae* (76). This protein is able to
526 bind to rapamycin (Sirolimus®) in both yeasts and mammalian cells promoting quiescence
527 (77, 78). In *C. neoformans*, rapamycin induces cell cycle arrest in the G1 phase (79).
528 Using STRING analysis of the protein-protein interactions provided evidence that the
529 regulation of fatty acids was the major metabolic pathway involved in VBNC. The regulation
530 of fatty acids is a phenomenon that occurs in *S. cerevisiae* quiescence by participating in
531 energy cellular homeostasis and membrane synthesis (29). In *Vibrio vulnificus*, changes in
532 fatty acid membrane composition contribute to maintaining the viability of the VBNC
533 state(33). A common feature among the metabolic fatty acids pathways is the participation
534 of acetyl-CoA (80). Acetyl-CoA is more than a cofactor in cell metabolism. It is central to the
535 physiology of mammalian cells (fatty acid metabolism, Krebs cycle, apoptosis, cell cycle,
536 damage- response DNA and epigenetics) (81). In *C. neoformans*, the genes of the three
537 principal production routes of acetyl-CoA in the cytosol are regulated (82): the β-oxidation of
538 fatty acids by the enzyme Mfe2, acetate by acetate synthase Acs1 and citrate by Acl1. Our
539 hypothesis isthat maintenance of fatty acid metabolism in hypoxia would allow the cells to
540 maintain membrane integrity and viability, with an increased mortality in deletion mutants
541 in key enzymes of the fatty acid pathway. If these results are in favor of the indispensability
542 of acetyl-CoA for the maintenance of *C. neoformans* infection, the relationship between

543 acetyl-CoA, pantothenic acid (PA) – a precursor of acetyl-CoA and dormant cells should be
544 further analyzed. The fact that PA was able to resuscitate VBNC cells, confirms the potential
545 relevance of the link made by the proteomic study between VBNC and metabolic pathways
546 of acetyl-CoA. Qualitative and quantitative changes in fatty composition occurs in *C.*
547 *neoformans* depending on the growth phase, with an increase during growth progression
548 (83). Bodipy staining showed no clear differences but demonstrated an important amount of
549 lipid droplets under each condition. KEGG pathway mapping of the 63 proteins regulated in
550 hypoxia showed an involvement of 8 proteins involved in fatty acid degradation. The 8
551 proteins involved were downregulated in hypoxia compared to normoxia. Another
552 reconstruction of the fatty acid degradation pathway using *Saccharomyces* genome
553 database involved 4 proteins also downregulated in hypoxia *FAA2* (CNAG_03019), *POX1*
554 (CNAG_07747), *FOX2* (CNAG_05721), *POT1* (CNAG_00490). The deletion mutants of these 9
555 proteins involved in both reconstructed pathways were tested in the *in vitro* model. The
556 mutants *pox1Δ*, *pot1Δ*, *CNAG_04688Δ* and *CNAG_00524Δ* had a decreased viability in
557 hypoxia compared to the parental strain KN99α strengthening the role of fatty acid
558 degradation in hypoxia and emphasizing the importance of downregulating fatty acid
559 degradation in VBNC phenotype. In *Candida albicans* macrophages internalization also
560 results in the induction of fatty acid degradation pathways (84) and similar patterns of
561 expression are observed in *C. neoformans* in the lungs of infected mice (85) and in response
562 to stress within macrophages and amoeba (86).
563 In summary, we describe conditions that promote *C. neoformans* to switch to a
564 homogenous population of viable but non culturable cells that can be considered dormant
565 and use those conditions to study the characteristic of these yeasts. VBNC cells manifest
566 what is potentially an extreme phenotype (dormancy) derived from stationary phase

567 (quiescence) but demonstrate the production of a very specific secretion pattern critical to
568 the pathobiology observed in the mammalian hosts. Our study identified genes involved in
569 the emergence and maintenance of the VBNC phenotype, which implicate a major role for
570 lipid metabolism in the emergence and maintenance of this state. The availability of
571 conditions that reliably induce VBNC provides a new research tool in the field of fungal and
572 *C. neoformans* biology to study the important features of dormancy and help understand
573 latency in cryptococcal pathogenesis.
574
575

576 **Material and methods**

577

578 *Culture media and strains*

579 *Cryptococcus neoformans* strains (Supplementary Table 8) were usually grown in liquid Yeast
580 Peptone Dextrose (YPD: 1% yeast extract (BD Difco, Le Pont de Claix, France), 2% peptone
581 (BD Difco), 2% D-glucose (Sigma, Saint Louis, Minnesota, USA)). Minimal medium (MM,
582 15mM D-glucose (Sigma), 10 mM $MgSO_4$ (Sigma), 29.4mM KH_2PO_4 (Sigma), 13mM Glycine
583 (Sigma), 3.0 µM Thiamine (Sigma), pH5.5) was used for specific experiments (25).

584 *In vitro generation of C. neoformans VBNC*

585 *Cryptococcus neoformans* H99O strain stored in 20% glycerol at -80°C was cultured on
586 Sabouraud agar plate at room temperature (step 1). After 2 to 5 days of culture, 10^7 cells
587 were suspended in 10 mL of YPD in a T25cm^3 flask and cultured for 22 hours at 30 °C, 150
588 rpm with lateral shaking until stationary phase (final concentration≈2×10^8/mL) (step 2). One
589 hundred µL of this first culture was added to 10 mL YPD (second culture) and incubated in
590 the same conditions until stationary phase (Step 3). Then, the flasks were placed in a
591 GENbag® (Biomérieux) anaerobic atmosphere generator to generate hypoxia and incubated
592 for 8 days in the dark at 30°C. These yeast cells are called 8D-HYPOx and then VBNC for
593 convenience. Control samples consisted of yeasts in stationary phase (step3, STAT) and
594 yeasts incubated under the same conditions but in normoxia are called 8D-NORMOx (Step 4)
595 (supplemental Figure 1). Of note, the atmosphere in the bag is enriched in CO_2 by the
596 biochemical process of oxygen depletion.

597

598 *Transmission electron microscopy*

599 Freshly harvested cells from STAT and 8D-HYPOx were fixed overnight at 4°C with 2.5%
600 glutaraldehyde in 0.1 M sodium cacodylate buffer (CB) at pH 7.2. Then samples were washed
601 in 0.1 M CB (pH 7.2) and post-fixed in a 1% osmium tetroxide in CB at room temperature for
602 1 h. We pre-embedded the cells in 4% agar type 9 : the cells were mixed with agar, spun-
603 down by gentle centrifugation and the pellet stored at 4°C until the agar had solidified. We
604 excised 2 mm^3 sections from agar block, and processed them in the automatic MicroWave
605 tissue processor for electron microscopy (AMW, Leica Microsystems, Vienna, Austria) as
606 recommended by the manufacturer: samples were washed with water and dehydrated with
607 graded ethanol concentrations (25–100%), followed by a mixture of graded resin Spurr Agar
608 low viscosity Resin (Agar scientific, Gometz la ville, France) concentration in ethanol (35-
609 100%). The embedded agar blocks were polymerize at 60°C for 48h. Ultrathin sections (70
610 nm) were performed with an ultramicrotome 'Ultracut UC7' (Leica Microsystems, Vienna,
611 Austria), stained with 4% uranyl acetate and Reynold's lead citrate onto 100 mesh copper
612 grids coated with a thin glow carbon film (S162-1, Oxford Scientific, Eynsham, UK) and then
613 observed under Tecnai SPIRIT (FEI-Thermofisher Company) at 120 kV accelerating voltage on
614 a camera EAGLE 4Kx4K (FEI-Thermofisher Company).

615

616 *Stainings and dyes*

617 Unless otherwise stated, yeasts were washed in phosphate buffered saline (PBS) twice
618 before and 3 times after staining. Stress response was assessed using 5-
619 chloromethylfluorescein diacetate (Cell tracker™ green CMFDA, Life Technologies). Yeasts
620 (10^6) were labeled with 3.3µM CMFDA in 500µL of PBS for 30 m at 37°C in the dark. Capsule
621 with E1 monoclonal antibody as described previously (87). Nuclei were stained using 4,6-

622 diamidino-2-phenylindole (DAPI, Invitrogen, Carlsbad). Yeasts (10^7) were fixed with 3.7%
623 paraformaldehyde for 30 m before staining with 0.5µg/mL of DAPI for 5 m. MDY-64
624 (Thermofischer Scientific, Waltham) was used to stain the intracellular vacuolar membranes
625 by incubating 10^7 yeasts for 5 m with 5µM MDY-64. Lipid droplets were stained using
626 Bodipy® 505/515 (Invitrogen, Carlsbad) at 1µg/mL with 10^7 cells for 20 m at room
627 temperature. To assess viability, LIVE/DEAD® Fixable Violet Blue (416 nm/451 nm) diluted at
628 1:1000 and 250 µL was added to 10^7 yeasts pellets and incubated at 30°C in the dark.
629 Controls were dead yeasts generated upon exposure to 200 mM of oxygen peroxide (H_2O_2)
630 at 37°C, under 650 rpm agitation or heat killed 1h at 65°C.
631 Yeasts were analyzed by fluorescence microscopy and pictures taken using an AxioCam MRm
632 camera (Carl Zeiss, Oberkochen) on interferential contrast microscope (DMLB2 microscope;
633 Leica, Oberkochen) with Zeiss Axiovision software.

634 Mitochondrial mass and polarization were evaluated with Mitotracker Green (Invitrogen) at
635 40 nM, JC-1 (Invitrogen) at 10µg/ml and TMRE at 200nM in PBS on 10^7 yeasts for 30 m at
636 37°C and then washes 3 times in PBS.
637 Reactive oxygen (ROS) nitrogen species (RNS) measurements were also performed.
638 Microplate wells were filled with 10^4 yeasts in 100 µL PBS. Briefly, the probes for ROS (2',7'-
639 dichlorofluorescein diacetate, Sigma) and RNS (dihydrorhodamine 123, Invitrogen) were
640 diluted at 100 µM in PBS and methanol, respectively, and 20 µL were added to wells of a
641 microtiter plate containing 10^4 yeasts in 100 µL of PBS. Hydrogen peroxide (4M) was
642 included as a positive control. The plates were incubated at 37°C in the dark. After 1 hour,
643 fluorescence was measured with a fluorometer (Fluoroskan ascent™ fluorometer, Thermos
644 Fischer Scientific, Waltham, MA, USA) using excitation 485 nm and emission wavelengths of
645 530 nm (88). The data were expressed as arbitrary units of fluorescence ±SD.
646
647 *Apoptosis assay*
648 Yeasts (10^7) were fixed for 1 h at room temperature in 3.2% formaldehyde (Sigma) in PBS.
649 After washings in PBS, yeasts were incubated in 1 mL of 5% 2-mercaptoethanol in SPM
650 buffer (Sorbitol 1.2 M (Sigma), potassium phosphate monobasic 50 mM (Sigma), magnesium
651 chloride hexahydrate 1 mM (Sigma), pH 7.3) for 1 hr at 37°C. Yeasts were washed once in
652 SPM buffer and incubated for 1h at 30°C in 1 mL of a solution containing 2 mg of Zymolyase
653 20T (Euromedex®), 100 mg of lysing enzymes from *Trichoderma harzianum* (Sigma) and 1 mg
654 of BSA (Sigma) in spheroplasting buffer (sorbitol 1 M (Sigma), sodium citrate tribasic
655 dihydrate 100 mM (Fluka), EDTA 10 mM (Sigma), pH 5.8). All these incubations were
656 performed in the dark with agitation at 650 rpm in a thermomixer. The spheroplasts were
657 then washed 3 times in SPM buffer-permeabilized by incubation in 1 mL of 0.1% triton X-100

658 (Sigma) in PBS for 2 minutes on ice and washed twice in PBS. TUNEL-Fluorescein (In Situ Cell
659 Death Detection Kit, Roche Life Science) was used to measure apoptosis at the single cell
660 level following manufacturer's recommendations. Yeasts were resuspended in 50 µL of
661 solution of 10% of TdT and 90% dye-coupled dUTP in PBS, incubated 1 h at 37°C and then
662 washed twice in PBS. Apoptosis control was generated by incubation of $3x10^7$ yeasts in 2
663 mM H_2O_2 for 3 h at 37°C. TdT was omitted for the negative control. In each run, yeasts
664 treated with DNAse (3 U/mL, Ambion®) were used as a TUNEL positive control.
665
666 *Flow cytometry measurements and cell sorting*
667 Flow cytometry was used to quantify MDY64 staining, viability and apoptosis assays, yeasts -
668 using the Guava easyCyte 12HT Benchtop Flow Cytometer® (Guava, MERCK, Kenilworth,
669 New Jersey).
670 Multispectral flow cytometry (ImageStreamX, Amnis Corporation) was used to quantify
671 mitochondrial fluorescence as described before (23, 87). For each population of interest, the
672 geometric mean was calculated using the IDEAS software.
673 In specific experiments, yeasts were sorted on a BD FACS aria™ II flow cytometer. The gating
674 strategy included the exclusion of the aggregates and the doublets. Subsequently, the
675 sorting was carried out according to the intensity of CMFDA in 3 populations ($CMFDA^{high}$,
676 $CMFDA^{medium}$ and $CMFDA^{low}$).
677
678 *Comparison of growth curves and statistical modelling*
679 Growth curves measurements were done using the Bioscreen® apparatus (Oy Growth Curves
680 Ab Ltd). Yeasts suspensions (300 µL at10^4/mL) were added to wells of a plate and incubated
681 for 2 to 5 days at 30°C with continuous, high amplitude and fast speed agitation. Optical

682 densities (OD) were recorded at 600nm every 20 minutes. The R software with the Grofit
683 plug-in (89) was used and for each replicate and in each condition, we adapted the best
684 mathematical model according to the AIC (Akaike Information Criterion). The two models
685 that best modeled the growth curves were the logistic and Richards modified, where λ
686 represents the length of lag phase or latency of growth, μ the growth rate, A the maximum
687 OD (concentration), ν the shape parameter and t the time of incubation.

$$Logistic: y(t) = \frac{A}{1 + exp^{(\frac{4\mu}{A}(\lambda - t) + 2)}}$$

$$Richards\ modified: y(t) = A\left(1 + \nu + \frac{\mu}{A}(1+\nu)^{1+1/\nu}(\lambda - t)\right)^{\frac{-1}{\nu}}$$

688 These formulas were written in Graphpad Prism v6.02 to allow curve extrapolation and
689 determination of the latency parameter λ.

690

691 *Culturability and reactivation experiments*

692 To assess basic culturability, the suspensions recovered at the end of the assay were
693 enumerated and 3000 cells, counted with the Guava easyCyte 12HT Benchtop Flow
694 Cytometer®, were plated in duplicates on YPD agar. The number of colony forming units
695 (CFUs) was recorded after 5 days of incubation at 30°C. The experiment was performed
696 twice. Results were expressed as mean percent culturability. To assess the ability of 8D-
697 HYPOx cells to reactivate, we determined the probability for a cell to grow by seeding, for
698 each condition, 576 wells (six 96-well plates) with 100 yeasts/well and counting the number
699 of positive wells at the end of the incubation time, taking into account the Poisson's law.
700 Plates were incubated 5 days at 30°C in an Infors HT® multitron pro at 150 rpm. Two
701 independent experiments were performed for each condition. The probability (p) of a cell to

702 grow was calculated using the following formula, where X represents the number of positive
703 wells, Y the number of wells seeded.

$$X \sim B(100, p) \quad p = 1 - (1 - \frac{X}{Y})^{\frac{1}{100}}$$

704 *Phagocytosis assay*

705 Interaction with macrophages was performed as described previously (90) using the J774 cell
706 line, the monoclonal anti-capsular polysaccharide antibody E1 as an opsonin (91), calcofluor-
707 stained yeasts and a yeasts: macrophages ratio of 5:1. Phagocytosis was assessed by flow
708 cytometry using the Guava easyCyte 12HT Benchtop Flow Cytometer® (Merck).

709

710 *Phenotypic microarrays*

711 Using phenotypic microarray technology (Biolog®, Hayward,CA) we analyzed the metabolic
712 capacities of yeasts incubated VBNC/8D-NORMOx (both with biological duplicates), using as
713 controls either STAT or dead cells (8 days in hypoxia in a YPD pH = 5) (only 3 conditions, i.e.
714 VBNC, 8D-NORMOx and control could be tested in each series). The Biolog® apparatus allows
715 quantitative measurement of the metabolism over time based on the physiological state of
716 the yeast cells independently of cell division and based on mitochondrial activity (proton and
717 electron generation) (92). Reduction of tetrazolium dye that absorbed charge produced by
718 cell respiration results in a purple color change that is recorded over time. The optical
719 density measured in the well provide information on the intensity of the corresponding
720 metabolic activity. The effect of carbon, nitrogen, phosphorus, and sulfur sources on the
721 physiological state of the cell and cell respiration was examined in response to various
722 osmotic conditions and to different pHs (plates PM1, PM2A, PM3B, PM4A, PM6, PM7 and
723 PM8). A tetrazolium dye reacting to the redox status of the well turns purple when

724 respiration takes place which has been shown to be a good proxy for the ability of strains to
725 grow on a substrate (93). Phenotype microarray was done according to instructions from the
726 manufacturer (Biolog, Hayward, CA) with the following exceptions. Briefly, ≈$7x10^8$ cells were
727 washed 3 times in PBS and then resuspend in 27 mL of PBS. For each condition, the analysis
728 was performed based on the results obtained after 6 days of incubation. Overall, 761
729 compounds were tested and 240 compounds that were positive in the dead cells condition
730 were excluded from the analysis. The heatmap and clustering of the 521 remaining
731 conditions were performed using R studio v1.1.456 with ggplot package. For the endpoint
732 comparison, only positive wells in each condition were compared (393 in STAT, 279 in VBNC
733 duplicate 1, 200 in VBNC duplicate 2, 454 in 8D-NORMOx duplicate 1 and 380 in 8D-
734 NORMOx duplicate 2).
735

736 *Mitochondrial nucleic acid quantification*

737 Cells suspensions corresponding to STAT or VBNC (1 mL each in biological triplicates) were
738 centrifuged at 4 000rpm for 5 m at 4°C before a flash freeze step in -80°C ethanol solution
739 and storage at -80°C before extraction. The RNA extraction protocol was adapted from (94).
740 Briefly, samples were lyophilized during 18h. RNAs were extracted in 3 successive steps: i)
741 extraction performed in Trizol reagent (Invitrogen TriReagent (Sigma-Aldrich, St-Louis MO
742 63103 USA)), ii) "separation" by adding chloroform (Invitrogen) iii) overnight isopropanol
743 precipitation at -20°C.

744 The DNA protocol extraction was a manual method based on 3 steps. Briefly, a first stage
745 consisted in lysing the cell pellets by beat beating with MagNA Lyser Instrument (Roche
746 Diagnostics; 2 rounds at 7 000 rpm for 45 s each) in a solution of 2% Triton X-100 (Sigma)
747 and 1% of SDS (Biosolve BV Chimie, 5555 CE Valkenswaard, The Netherlands), NaCl 100mM;

748 Tris 10mM pH 8.0; EDTA 1mM. Then, an extraction step in phenol/chloroform solution
749 (Phenol:Chloroform:isoamyl alcohol pH 8.0, 1 mM EDA (Sigma-Aldrich, St-Louis MO 63103
750 USA) and a precipitation step in absolute ethanol and 5M of ammonium acetate solution
751 were done. RNAs and DNAs were quantified using the Nanodrop Spectophotometer
752 (ThermoFisher, Scientific, Inc.). All extracts were stored at -80°C before analysis.
753
754 *qPCR and reverse transcriptase qPCR*
755 Briefly, mtLSU primers were designed with Primers. 3 vs 4.1.0, while all other specific
756 primers were designed to be compatible with the Human Universal Probe Library set (90
757 probes, octamer, Roche Diagnostics) (Supplementary Table 9) (23). All reverse transcriptase
758 qPCR assays for a given target were performed simultaneously for all samples using the
759 LightCycler Multiplex RNA Virus Master Kit (Roche diagnostics). Each sample was normalized
760 with the geometric mean of the quantification cycle (Cq) of the corresponding GAPDH and
761 ACT housekeeping genes expression (95) and fold changes calculated according to Pfaffl
762 after determining the efficiency of each PCR assay (96).
763
764 *Secretome and proteome analysis*
765 Three biological replicates were performed kinetically upon incubation D4, D6 and D8 in
766 hypoxia and normoxia starting from step3 (Supplementary Figure 1) corresponding to
767 stationary phase (STAT). The suspensions were centrifuged at 4000rpm and the
768 supernatants (secretome) filtrated through a 0.22 µM membrane (Millex GV, Merck
769 Millipore, Burlington, USA). The corresponding cell pellets (proteome) were extracted in
770 parallel. For each biological replicate, three technical replicates were pooled to increase the
771 amount of recovered proteins for the supernatants.

772 All samples (supernatant or pellet) were lyophilized overnight after flashed freezing in liquid
773 nitrogen. We then adapted a protocol established to purify a sample rich in carbohydrates
774 (97). The lyophilized samples were resuspended in 0.5 mL of sterile milliQ water and the
775 following 3 steps-protocol was done: i) the samples were precipitated at 4°C by addition of 1
776 mL of 10% trichloroacetic acid (TCA) in acetone (kept at-20°C) followed by incubation for 5
777 m. After centrifugation at 20000g for 10 minutes at -20°C, the pellet was resuspended in
778 100% acetone with 10mM dithiothreitol (DTT), washed twice in this solution, and air dried;
779 ii) the pellet was then solubilized in sodium dodecyl sulfate (SDS) extraction buffer
780 containing 1% SDS, 0.15 M Tris HCl pH=8.8, 0.1M DTT, 1 mM ethylene diamine tetra acetic
781 acid (EDTA), 2 mM phenylmethylsulfonyl fluoride (PMSF), and incubated for 1 h at room
782 temperature and vortexed every 20 m. A 15000g centrifugation for 10 m at room
783 temperature allowed recovery of the supernatant; iii) Phenol was added at equal volume to
784 the supernatant and the tube was vortexed for 3 m. After centrifugation at 20000 g for 5 m
785 at room temperature, the denser phenolic phase was recovered in the lower part. An equal
786 volume of washing solution (Tris HCl pH 8.0, 10 mM, 1 mM EDTA, 0.7 M sucrose) was added
787 and the tube vortexed for 3 m. The phenolic phase was then recovered on the upper part
788 and transferred to a new tube. Then, 0.1M ammonium acetate in methanol (-20°C) was
789 added and the mixture stored at -20 ° C for 30 m. The precipitate was pelleted by 20000g
790 centrifugation for 10 m at -20°C, and washed first with 0.1M ammonium acetate in methanol
791 and then with 100% acetone. After a last centrifugation step (20000 g for 10 m at -20°C), the
792 pellet was air-dried and resuspended in 350 µl of denaturing buffer (8M urea, 100 mM
793 TrisHCl pH 8.0). Two µL of each sample were then used for dosage with the Biorad DC®
794 dosing kit according to the manufacturer's recommendations. The remaining solution was
795 stored at -80°C until analysis.

796

797 *High pressure liquid chromatography coupled to tandem mass spectrometry* (nano HPLC
798 MS/MS)

799 In solution protein digestion. Samples were re-suspended in 350 µL 8 M urea/ 100 mM Tris
800 HCl pH 8.5 after TCA/acetone precipitation and phenol extraction. Briefly, samples were
801 reduced with 5 mM tris(2-carboxyethyl)phosphine (TCEP) for 30 m at room temperature and
802 alkylated with 10 mM iodoacetamide for 30 m at room temperature in the dark. Then,
803 proteins were firstly digested for 5 hrs at 37°C with 250 ng rLys-C Mass Spec Grade
804 (Promega, Madison, USA). Samples were then diluted 4-fold with 100 mM Tris HCl pH 8.5 to
805 reach a concentration of 2M urea and then re-incubated overnight at 37°C with 1 µg
806 Sequencing Grade Modified Trypsin (Promega, Madison, WI, USA). A second incubation with
807 the same amount of trypsin (5 h at 37°C) was performed to ensure a complete digestion.
808 Digestion was stopped by adding formic acid to 5 % final concentration and peptides were
809 desalted and concentrated on Sep-Pak C_{18} SPE cartridge (Waters, Milford, MA, USA)
810 according to manufacturer's instructions.

811 Mass spectrometry data analysis. Tryptic peptides were analyzed on a Q Exactive Plus
812 instrument (Thermo Fisher Scientific, Bremen) coupled with an EASY nLC 1000
813 chromatography system (Thermo Fisher Scientific). Sample was loaded on an in-house
814 packed 30 cm nano-HPLC column (75 µm inner diameter) with C18 resin (1.9 µm particles,
815 100 Å pore size, Reprosil-Pur Basic C18-HD resin, Dr. Maisch GmbH, Ammerbuch-Entringen,
816 Germany) and equilibrated in 98 % solvent A (H2O, 0.1 % FA) and 2 % solvent B (ACN, 0.1 %
817 FA). Peptides were first eluted using a 2 to 18 % gradient of solvent B during 112 m, then a
818 18 to 30 % gradient of solvent B during 35 m, a 30 to 45 % gradient of solvent B during 15 m
819 and finally a 45 to 60 % gradient of solvent B during 5 m all at 250 $nL.m^{-1}$ flow rate. The

820 instrument method for the Q Exactive Plus was set up in DDA mode (Data Dependent
821 Acquisition). After a survey scan in the Orbitrap (resolution 70 000), the 10 most intense
822 precursor ions were selected for HCD fragmentation with a normalized collision energy set
823 up to 27. Charge state screening was enabled, and precursors with unknown charge state or
824 a charge state of 1 and >7 were excluded. Dynamic exclusion was enabled for 45 s.

825 Data processing and analysis. All data were searched using Andromeda (98)with MaxQuant
826 software (99, 100) version 1.5.3.8 against the H99 strain proteins database (6980 entries)
827 and the H99 strain mitochondria proteins database (13 entries) concatenated with usual
828 known mass spectrometry contaminants and reversed sequences of all entries. Andromeda
829 searches were performed choosing trypsin as specific enzyme with a maximum number of
830 two missed cleavages. Possible modifications included carbamidomethylation (Cys, fixed),
831 oxidation (Met, variable) and Nter acetylation (variable). The mass tolerance in MS was set
832 to 20 ppm for the first search then 6 ppm for the main search and 10 ppm for the MS/MS.
833 Maximum peptide charge was set to seven and five amino acids were required as minimum
834 peptide length. The "match between runs" feature was applied for all samples with a
835 maximal retention time window of 2 m. One unique peptide to the protein group was
836 required for the protein identification. A false discovery rate (FDR) cutoff of 1 % was applied
837 at the peptide and protein levels.

838 MaxLFQ, Maxquant's label-free quantification (LFQ) algorithm was used to calculate protein
839 intensity profiles across samples (101). An LFQ value was assigned when the protein had at
840 least 2 peptides, of which 1 was unique. The median reproducibility by samples for
841 secretomic was 87.1% [82.5-90.6] and 86.5% [84.1-88.9] for cellular proteins.

842 Statistical analysis of differentially expressed proteins. Proteins for which we had no value
843 for a given condition and time were removed. Remaining missing values were imputed using
844 the structured least Squares algorithm (package imp4p) (102).
845 To get a global overview of the data, a principal coordinate analysis (PCoA) or a principal
846 component analysis (PCA) was used (103). The differential analysis was done with the linear
847 model approach proposed by the package R limma (v3.30.13) (104). We defined a model
848 that included condition (hypoxia or normoxia), time (D0=STAT, D4, D6, and D8) and replicate
849 (1 to 3) variables as main effects and interactions between conditions and times as well as
850 conditions and replicates. The latter interaction was useful to model the pairing between
851 measurements corresponding to the same condition. The proteins differentially expressed
852 over time are selected according to the following criteria: change with respect to the initial
853 value of log2 and a $p < 0.05$. The p-values obtained were adjusted by the method of
854 Benjamini-Hochberg (105).
855
856 *Analysis of enriched processes for secreted proteins "Gene Ontology (GO) enrichment*
857 *analysis"*
858 The fungifun2 v2.2.8 BETA (106) site (https://elbe.hki-jena.de/fungifun/fungifun.php) was
859 used by selecting for each sample of secreted proteins the corresponding cellular protein
860 background and to study the cellular proteins the background was the whole database. For
861 this analysis we selected only the proteins identified in the 3 replicates per condition. For
862 each analysis, the following options were selected: p value <0.01, hypergeometric
863 distribution test, over-representation, p-read corrected by Benjamini-Hochberg, only directly
864 annotated association. Hypothetical proteins, which constitute 20-30% of the annotated
865 proteins, were not represented.

866

867 *Venn Diagram*

868 Venn diagram was generated using Jvenn (107)
869 (http://jvenn.toulouse.inra.fr/app/index.html) with proteins only present in the 3 replicates
870 for each condition (secretome and proteome).

871

872 *Protein/protein interactions analysis*

873 Analysis of protein-protein interactions of intracellular proteins regulated during hypoxia.
874 STRING v10.5 software (https://string-db.org) was used (108). As this software used the
875 strain JEC21 annotation, the list of orthologous proteins was transferred from H99 to JEC21
876 with a 62/63 protein match. The nodes directly related to the input were indicated with
877 colors while the nodes of a higher iteration/depth were indicated in white.

878

879 *KEGG pathway mapping and fatty acid degradation cycle reconstruction.*

880 KEGG pathway database (https://www.genome.jp/kegg-bin) was used to map the pathways.
881 It was rendered with the intracellular proteins significantly and differently produced in
882 hypoxia: 63 proteins were transferred from H99 to JEC21. Nineteen proteins belonged to
883 general metabolic pathway and more precisely 8 to fatty acid degradation ("map" pathways
884 were not colored, *Cryptococcus*-specific pathways were colored green, entries were colored
885 red). Another fatty acid degradation cycle was reconstructed from yeast genome database
886 cycle (https://www.yeastgenome.org/) and the corresponding proteins were found in
887 *Cryptococcus neoformans* H99 genome using BLAST
888 (https://blast.ncbi.nlm.nih.gov/Blast.cgi).

889

890 *RNAseq analysis*

891 For transcriptome analysis, yeasts incubated in 8D-HYPOx/8D-NORMOx, as well as STAT and
892 logarithmic (LOG) phase yeasts were studied in triplicates for two different sets, one
893 containing spiked *Saccharomyces cerevisiae* organisms (w_spike) and one with *C.*
894 *neoformans* cells only (w/o_spike). The former strategy was used to obtain an internal
895 standard of the level of expression of the whole transcripts and adjust the level of
896 expression of each gene to that of the constant expression of *S. cerevisiae*. In each spiked
897 sample, 15% of LOG phase *S. cerevisiae* cells were added to *C. neoformans* cells. Triplicates of
898 yeasts suspensions in the different conditions (total of $2.55x10^8$ *C. neoformans* cells) were spiked
899 (w_spike) or not (w/o_spike) with $4.5x10^7$ cells (representing then 15% of the cells) of *S. cerevisiae*
900 cells (culture in exponential phase). All samples were then processed as described above in the
901 "*Mitochondrial nucleic acid quantification*" section.

902 We used 1 µg of total RNA to purify polyadenylated mRNAs and to build an RNA library,
903 using TruSeq Stranded mRNA Sample Prep Kit (Illumina, #RS-122-9004DOC) as
904 recommended by the manufacturer. Directional library was checked for concentration and
905 quality on RNA chips with the Bioanalyzer Agilent. More precise and accurate quantification
906 was performed with sensitive fluorescent-based quantitation assays ("Quant-It" assays kit
907 and QuBit fluorometer, Invitrogen). Samples were normalized at 2 nM concentrations,
908 multiplexed 4 samples per lane and then denatured at a concentration of 1 nM using 0.1 M
909 NaOH at room temperature. Each sample was finally loaded on the flowcell at 9 pM.
910 Sequencing of the 24 samples was performed on the HiSeq 2500 sequencer (Illumina) in 65
911 bases single-end mode.

912

913 *QC, mapping, counting, and global transcriptome level analysis*

914 Reads were cleaned of adapter sequences and low-quality sequences using cutadapt version
915 1.11 (Marcel Martin. Cutadapt removes adapter sequences from high-throughput
916 sequencing reads (109)). Only sequences at least 25 nucleotides in length were considered
917 for further analysis. STAR version 2.5.0a (110), with default parameters, was used for
918 alignment on the reference genome (PRJNA411 from NCBI Bioproject). Read counts per gene
919 were measured using featureCounts version 1.4.6-p3 (111) from Subreads package
920 (parameters: -t gene -s 0). Results are summarized using multiqc version 0.7 (112). Count
921 data were analyzed using R version 3.3.1 and the Bioconductor package DESeq2 version
922 1.12.3 (113). Normalization and dispersion estimations were performed with DESeq2 using
923 the default parameters but statistical tests for differential expression were performed
924 without applying the independent filtering algorithm.
925 For w/o_spike samples, a generalized linear model was set in order to test for the
926 differential expression between STAT, 8D-HYPOx/8D-NORMOx and LOG conditions. For each
927 pairwise comparison, raw p-values were adjusted for multiple testing according to the
928 Benjamini and Hochberg (BH) procedure and genes with an adjusted p-value lower than 0.01
929 were considered differentially expressed.
930 For w_spike samples, mean normalized counts were calculated and the rank of each gene
931 determined for each gene in each condition. High and low rank values corresponded to
932 genes with the highest and lowest expression relative to spiked RNA, respectively.
933
934 *Differential expression analysis*
935 To identify the expression differences across conditions, the read counts were filtered and
936 normalized using the R package "DESeq2". Genes with read counts below a threshold of 10
937 in all samples were filtered out. After normalization of read counts, differentially expressed

938 genes for each condition were identified using the generalized linear model, which perform
939 pairwise comparisons among each of the conditions (STAT, 8D-HYPOx, 8D-NORMOx and
940 LOG). Genes passing the threshold, (FDR <5%), were considered significantly differentially
941 expressed and were then considered to be up or down-regulated according to the direction
942 of the fold change. The k-means clustering analyses were performed using R tools, "kmeans"
943 and "heatmap.2". To discover the underlying pathways of these differentially expressed
944 genes, we also carried out functional annotation analysis by summarizing the data, including
945 known H99 gene annotation, *S. cerevisiae* gene ortholog, Gene Ontology (GO), KEGG
946 pathway, and pfam domain, from FungiDB database (114). GO enrichment and KEGG
947 pathway enrichment for these genes were then assessed by using Fisher's Exact Test with
948 multiple testing correction of FDR threshold at 5%. Furthermore, conserved domains of each
949 *C. neoformans* gene were assessed by using the amino acid sequence to search the NCBI
950 Conserved Domain Database (CDD) (115). The presence of signal peptide sites was predicted
951 by SignalP 4.1 (116).
952
953 *Statistical analysis*
954 The statistical tests used for the comparisons between the different conditions were t-test,
955 Mann Whitney, Wilcoxon tests according to the distribution of the data.
956
957 *Data access*
958 All RNA sequence data from this study have been submitted to NCBI
959 (https://www.ncbi.nlm.nih.gov/geo) under accession number GSE118549.
960 The mass spectrometry proteomics data have been deposited to the ProteomeXchange
961 Consortium via the PRIDE partner repository with the dataset identifier PXD012570

962 (https://cran.r-project.org/).

963 **Figure legends:**

964

965 **Figure 1: *Cryptococcus. neoformans* incubated for 8 days in hypoxia were intact with a low**
966 **stress response and delayed growth. A.** Cells recovered after 8 days in hypoxia (8D-HYPOx)
967 were compared to those incubated in normoxia (8D-NORMOx), to stationary phase
968 (STAT=D0) cells. DAPI staining (DAPI) showed intact cells with a nucleus; labeling with the E1
969 (IgG1) anti-capsular antibody showed similar pattern in all conditions; vacuolar staining
970 MDY-64 showing more intense staining in 8D-HYPOx/8D-NORMOx than STAT yeasts;
971 LiveDead® violet staining showing high viability in 8D-HYPOx (HK = heat killed yeasts, BF =
972 bright field, bar = 10µm) **B.** Transmission electron microscopy of 8D-HYPOx cells and STAT
973 cells showing the presence of large intracytoplasmic vacuoles (bar = 0.5 µm) **C.** CMFDA
974 labeling showed that 8D-HYPOx yeasts had decreased stress response over time compared
975 to 8D-NORMOx. **D.** Latency parameter (λ) was calculated from growth curves in the different
976 conditions. **E.** Latency of growth increased over time for 8D-HYPOx yeasts compared to STAT
977 and 8D-NORMOx cells (*p <0.01). Experiments were done in biological and technical
978 triplicates. Each dot represents the value of λ for each replicate. Medians and interquartile
979 range (IQR) are represented.

980

981 **Figure 2: *Cryptococcus neoformans* incubated for 8 days in hypoxia harbor a homogenous**
982 **phenotype of viable but non-culturable cell (VBNC). A.** Kinetics analysis using multispectral
983 flow cytometry with viability (LIVE/DEAD®) and apoptosis (TUNEL) staining showing a
984 homogenous population of viable yeasts after D8 in hypoxia and a heterogeneous
985 population in normoxia with a mixture of viable, apoptotic like and dead yeasts. The
986 experiment was done in triplicate. Viable non-apoptotic cells represented a median

987 proportion of 87.7% [84.2-91.2] at D2, 74.6% [70.5-78.8] at D4, 90.9% [89.7-92.2] at D6, and
988 98.9% [98.8-99.0] at D8 in hypoxia, 89.4% [88.4-90.5] at D2, 83.5% [83.1-83.9] at D4, 59.6%
989 [59.2-60.0] at D6, 63.6% [62.2-65.0] at D8 in normoxia and 98.7% [98.4-99.0] in STAT.
990 Apoptotic-like cells represented a median proportion 9.9% [6.2-13.8] at D2, 21.4% [17.5-
991 25.4] at D4, 7.2% [6.5-7.9] at D6, 1.1% [0.9-1.2] at D8 in hypoxia, 8.8% [7.7-10.0] at D2,
992 13.8% [13.6-14] at D4, 35.8% [34.9-36.7] at D6, 32.9% [31.0-34.9] at D8 in normoxia and
993 0.8% [0.5-1.6] in STAT cells. The dead cells median proportion was 0.5% [0.4-0.6] in STAT,
994 1.9% [1.8-2.0] at D2, 2.7% [1.7-3.7] at D4, 1.8% [1.6-2.0] at D6, 0% at D8 in hypoxia1.7% [1.6-
995 1.8] at D2 , 2.2% [1.8-2.6] at D4, 5.0% [4.2-5.9] at D6, 3.2% [3.0-3.4] at D8 in normoxia.
996 **B.** Culturability was followed over 8 days by plating yeasts on Sabouraud agar (colony
997 forming unit method). The proportion of culturable cells decreased significantly over time
998 under hypoxia and significantly more than in 8D-NORMOx. Compared to STAT condition
999 (110.5% [108-113]), the median culturability was (33.2% [31.1-35.2] at D2, 4.3% [4.0 -4.6] at
1000 D4, 0.8% [0.5-1.0] at D8) in hypoxia and (28.6% [17.2-40.0] at D2, 20.3% [17.9-22.8] at D4
1001 and 17.5% [15.4-19.7] at D8 in normoxia cells) (* $p<0.01$).
1002 **C.** Cell sorting according to the CMFDA intensity allowed showing a latency of growth after
1003 8D-HYPOx and was increased regardless of the stress response and comparable in the three
1004 populations (low, medium, high) to that of the unsorted population (bulk) compared to 8D-
1005 NORMOx and STAT: $CMFDA^{low}$ (2520 m [2257-2831]), $CMFDA^{medium}$ (2401 m [2276-2553])
1006 and $CMFDA^{high}$ (2394 m [2129-2627]) was not significantly different from unsorted cells
1007 (2269 m [2059-2344]) ($p>0.01$) although significantly different from 8D-NORMOx (1427 m
1008 [1407-1462]) and STAT (1013 m [1107-1036]) conditions (* $p<0.01$). Two independent
1009 experiments were pooled. Mean culturability (% mean CFU after plating) reported below the
1010 plots was comparable in all hypoxia populations and lower than in the other conditions. The

1011 ratio of positive wells/seeded wells are reported above the plots for each population
1012 recovered at the end of the growth curve measurement. **D.** Proposed model for the
1013 evolution of yeasts phenotypes upon incubation in hypoxia or normoxia leading to the
1014 generation of a VBNC phenotype after 8D-HYPOx.

1015

1016 **Figure 3: *Cryptococcus neoformans* incubated for 8 days in hypoxia were reactivated by**
1017 **pantothenic acid (PA) and culturable cells were rewired by minimal medium (MM)**
1018 **dilution.**

1019 Growth curves were determined for STAT or cells incubated 8D-HYPOx. Latency and growth
1020 rate (slope) were determined in different conditions. Experiments were always repeated
1021 twice. Graph includes dot for the replicates, as well as median ± IQR (*p<0.01 compared to
1022 control in the same condition). **A.** The dilution of minimal medium from 100% to 10%
1023 (diluted MM) resulted in a progressive decrease of latency in 8D-HYPOx cells and to a lesser
1024 extend in STAT cells. (*p <0.01 compared to 100%MM). Two independent experiments were
1025 pooled. Each point represents the latency/well in two (STAT n=5, 8D-HYPOx n=15) **B.** 100-
1026 fold dilution of pantothenic acid (starting at 125 µM) were added to the suspension prior to
1027 growth curve determination. Pantothenic acid significantly decreased the latency at a
1028 concentration of $1.25x10^{-2}$ µM or more in 8D-HYPOx and to a lesser extend in STAT cells (*
1029 p<0.01). Two independent experiments were pooled. Each point represents the latency/well
1030 in two (STAT n=9, 8D-HYPOx n=6). **C.** Growth rate was significantly decreased in 20%MM and
1031 10%MM in 8D-HYPOx **D.** A significantly increased growth rate was observed after addition of
1032 PA (1.25 µM or more) to 8D-HYPOx cells and at all concentrations for STAT. **E.** The addition
1033 of pantothenic acid at 125µM but not the dilution of MM increased the culturability of 8D-
1034 HYPOx based on the observation of the number of positive wells (100 cells per well) and the

1035 calculation of the probability of one cell to grow. Each dot represents the calculated
1036 culturability. Two independents experiments are pooled. **F.** Proposed model for the effect of
1037 hypoxia and nutrient depletion. From now on, 8D-HYPOx are called VBNC (Viable but not
1038 culturable cells). After 8 d of incubation in hypoxia and nutrient depletion, the decrease in
1039 latency observed upon addition of pantothenic acid on VBNC is explained by the reactivation
1040 of VBNC to culturable cells (increased culturability) and by the increased growth rate of
1041 culturable cells (increased slope). The decrease in latency observed upon dilutions of MM
1042 (decreased nutrient availability) is explained by a faster rewire of the culturable cells
1043 (decreased latency corresponding to decreased time to resume growth) without increased
1044 culturability or growth rate.
1045
1046 **Figure 4: Phenotypic array analysis of VBNC showed a lower metabolic activity.** We used
1047 the Biolog® technology to explore the metabolic requirements of VBNC compared to STAT
1048 and 8D-NORMOx cells. We selected 8 plates and 761 different metabolites to scan the ability
1049 of substrates to be used as an energetic source. The respiratory activity (measurement of
1050 tetrazolium reduction in arbitrary units) was compared at the end of the incubation (6 days).
1051 Two biological replicates (1 and 2) were done for the VBNC/8D-NORMOx conditions. **A.** The
1052 heatmap of 521 selected compounds showed that VBNC exhibited a different metabolic
1053 profile than STAT and 8D-NORMOx. **B.** The final endpoint analysis of the level of tetrazolium
1054 reduction revealed a lower activity for VBNC cells compared to cells in other conditions.
1055 VBNC and 8D-NORMOx conditions were done in duplicate (* $p<0.01$).
1056
1057 **Figure 5: Mitochondria of VBNC were depolarized with an increased mass and gene**
1058 **expression. A.** Mitochondria mass, and polarization were assessed in VBNC, 8D-NORMOx,

1059 STAT and heat killed yeasts using Mitotracker green and TMRE and JC-1 stainings,
1060 respectively and the ImageStream technology. In 8D-HYPOX (red histogram), the Mitotracker
1061 staining is high, TMRE low and JC-1 high compared to STAT (blue histogram). **B.** Microscopic
1062 visualization with Imagestream of the Mitotracker and TMRE stainings in VBNC and STAT
1063 yeasts, showing the contrast in the intensity of the stainings between conditions. **C.**
1064 Expression of five mitochondrial genes, cytochrome B (CYTb), ATP synthase 6 (ATP6), NADH
1065 deshydrogenase (NADH), mitochondrial large sub unit (mtLSU), and cytochrome oxidase
1066 (COX1) as expressed as the fold change to the geometric mean of the expression of GAPDH
1067 and ACT1 housekeeping genes. The expression of CYTb, NADH, mtLSU and COX1 is
1068 significantly increased in VBNC compared to STAT (* p=0.029).
1069
1070 **Figure 6: Secretome and proteome qualitative analysis showed specific features in VBNC.**
1071 **A.** Venn diagram of cellular and secreted proteins in stationary phase (STAT), VBNC and
1072 control. Six secreted (clear dashed blue) and 103 cellular (deep blue) proteins were detected
1073 specifically in VBNC. Six were secreted only in STAT (grey dashed line) and 150 were
1074 detected in cellular protein only (dark line), 16 were secreted (pink dashed line) and 75
1075 cellular (red line) only in 8D-NORMOx. Only proteins present in the 3 replicates for each
1076 condition were selected and compared. **B.** GO enrichment analysis of secreted proteins
1077 showed specific profile in VBNC. The major biological processes enriched in VBNC were
1078 translation, metabolic process of carbohydrates and glycolytic biological processes whereas
1079 oxidation-reduction was mainly enriched in 8D-NORMOx. **C.** GO enrichment analysis of
1080 cellular proteins showed similar profiles in VBNC and 8D-NORMOx with an enrichment for
1081 translation and oxidation-reduction.
1082

1083 **Figure 7: Secretome (A,B) and proteome (C,D) quantitative analysis showed an**
1084 **independent and specific kinetic evolution associated with VBNC generation.** Principal
1085 coordinate analysis (PCoA) of secreted **A.** or cellular **C**. proteins and heatmap obtained by
1086 Limma analysis of secretome **B.** and proteome **D.** data. For the secretome, 85 proteins were
1087 differentially expressed overtime, including 49 significantly overexpressed in control and 36
1088 in hypoxia. For the proteome, 63 cellular proteins were differentially expressed during
1089 kinetics including 47 significantly overexpressed in normoxia and 16 in hypoxia. Inversely of
1090 **B**, Data sets **D** showed that the STAT and hypoxia are closer than to normoxia.
1091
1092 **Figure 8: The fatty acid degradation pathway is required for VBNC viability. A**. The Search
1093 Tool for the Retrieval of Interacting Genes/Proteins (STRING) allowed the visualization of
1094 predicted protein-protein interaction for the 63 proteins hypoxia-regulated identified. It
1095 revealed an impact of hypoxia on diverse proteins as well as a prominent influence on fatty
1096 acids metabolism. Different clusters were identified from the network mapping: pathways
1097 linked to fatty acid metabolism (valine leucine and isoleucine degradation, propanoate
1098 metabolism, fatty acid degradation and metabolism) and to carbon metabolism. **B.** Lipid
1099 droplets stained with Bodipy® 505/515 showed the presence of lipid droplets in all
1100 conditions. **C.** Eight entries among 63 proteins regulated in hypoxia mapped the fatty acid
1101 degradation by using KEGG pathway mapping ("map" pathways are not colored,
1102 *Cryptococcus*-specific pathways are colored green, the 8 entries are colored red) **D.** The fatty
1103 acid degradation pathway reconstructed from *Saccharomyces cerevisiae* pathway. FA (Fatty
1104 acid), FAA2 (Acyl Coa synthetase), POX1 (Fatty-acyl coenzyme A oxidase), FOX2 (3-
1105 hydroxyacyl-CoA dehydrogenase, 3-hydroxyacyl-CoA dehydrogenase), POT1 (3-oxoacyl CoA
1106 thiolase). **E.** Nine deletion mutants from fatty acid degradation pathway selected from KEGG

1107 database and the orthology with *S. cerevisae* were assessed for their ability to survive
1108 hypoxia in the model. The ratio of living cells for the mutants to that obtained with KN99α
1109 was determined based on LIVE/DEAD staining after VBNC generation. A significant decreased
1110 percentage of viable cells was measured for 04688Δ, 00490Δ, 07747Δ and 00524Δ (*p<0.01)
1111

1112 **Figure 9: The global transcription is decreased in VBNC but remains specific. A.**
1113 Transcriptional level of all conditions relative to that of *S. cerevisiae* spiked in each sample
1114 showed a significant decrease in VBNC compared to other conditions **B.** PCA analysis of the
1115 global transcriptomic data (wo_spikes) suggested that logarithmic cells (LOG) evolve to STAT
1116 which evolve to VBNC or 8D-NORMOx **C.** GO enrichment analysis of upregulated transcript
1117 (wo_spike) compared to STAT. The major enriched biological processes were signal
1118 transduction, ATP synthesis coupled proton transport in VBNC and protein folding, oxidation
1119 reduction process and response to stress in 8D-NORMOx. **D.** Heat map of the gene
1120 expression revealed the presence of 7 clusters displaying different expression patterns for all
1121 conditions. The color key represents normalized transformed counts**.**

1122 **Supplementary figures legends**

1123

1124 **Supplementary figure 1: *In vitro* protocol for dormant cell generation.** The protocol
1125 followed several steps: (1) *Cryptococcus neoformans* cells of a stock culture frozen at -80°C
1126 were grown on Sabouraud agar plate for 2 to 5 days at room temperature; (2) 10^7 cells were
1127 then suspended in 10 mL yeast extract peptone dextrose 2% (YPD) and incubated with
1128 lateral shaking (150 rpm) at 30°C for 22 hours (stationary phase-STAT); (3) 100 µl, $2x10^7$ cells

1129 were incubated again until the STAT and then placed in hypoxia or normoxia in the dark at
1130 30°C (4) for up to 8 days when the resultant cells in hypoxia and normoxia were analyzed.
1131
1132 **Supplementary figure 2: Cell body size, capsule and cell wall thickness. A.** Median cell sizes
1133 were similar in 8D-HYPOx, 8D-NORMOx and STAT. **B.** Median capsule size was lower in 8D-
1134 HYPOx, 8D-NORMOx compared to STAT (*p<0.01, 100 cells measured). **C.** Cell wall was
1135 thicker in 8D-HYPOx compared to STAT (*p=0.0152, 50 cells measured).
1136
1137 **Supplementary figure 3: Flow cytometry diagrams assessing capsular, vacuolar structure**
1138 **and viability in STAT, 8D-NORMOx and 8D-HYPOx. A.** Histograms of fluorescence intensity
1139 showing no difference in binding pattern after staining with anti-capsular polysaccharide E1
1140 antibody **B.** More intense vacuolar staining with MDY-64 in 8D-HYPOx, 8D-NORMOx
1141 conditions (one representative experiment out of the 3 independent experiments performed
1142 is shown) **C.** Viability was assessed by membrane permeability staining (LIVE/DEAD, LVD)
1143 showing almost 99% of live cells in STAT cells and 100% of dead cells in heat-killed cells (Left
1144 panel). Plasma membrane was intact for more (87.2% [83.2-88.6]) cells in 8D-HYPOx, than in
1145 8D-NORMOx (53.8% [50.9-60.5]). Experiments were done in triplicate and a representative
1146 diagram is shown.
1147
1148 **Supplementary figure 4: Latency was influenced by medium and cell concentration**
1149 Growth of STAT and 8D-HYPOx cells was assessed using the BioScreen® apparatus. Serial
1150 dilutions of 8D-HYPOx and STAT cells increased the latency in YPD (**A**) and in MM (**B**). Latency
1151 curves extrapolations showed for both STAT and 8D-HYPOx cells, global latency was
1152 decreased in YPD compared to MM. Each point represents the median ± IQR of the latency

1153 of 3 independent experiments. **C.** Experimental set up used for the determination of the
1154 probability of growth per cell (culturability). Hundred yeasts cells per well were plated in 96-
1155 well plates in each condition (MM at 10 or 100% ± pantothenic acid (PA) at 125µM). The
1156 number of positive wells per plate were determined and the probability of growth per plate
1157 was calculated (see M&M section) **D.** 8D-HYPOx were exposed to macrophages during two
1158 hours in the presence of opsonin. Culturability was similar in phagocytosed 8D-HYPOx cells
1159 compared to controls. Each dot represents the calculated culturability. Two independents
1160 experiments are pooled.

1161

1162 **Supplementary figure 5: ROS and RNS production were decreased in VBNC**

1163 Testing the ROS and RNS in VBNC vs STAT cells found a slight decreased in VBNC. ROS (left
1164 panel) and RNS (right panel) productions were measured using fluorescence probes and
1165 were significantly lower in VBNC compared to STAT cells respectively (*$p<0.01$). As expected,
1166 the addition of H_2O_2 as a positive control increased ROS and RNS levels.

1167

1168 **Supplementary figure 6: The number of identified proteins evolved differently between**
1169 **secreted and cellular proteins in hypoxia and normoxia.** The number of secreted protein
1170 number significantly decreased over time in hypoxia (* $p<0.01$) (**A**) while the protein
1171 concentration tended to increase in normoxia (**B**). The number of cellular proteins remained
1172 stable in both conditions (**C**) while the protein concentration tended to increase (**D**). The
1173 experiments were done in triplicates (median±IQR].

1174

1175 **Supplementary figure 7: Venn diagrams of STAT, VBNC and 8D-NORMOx for secreted and**
1176 **cellular proteins. A.** A hundred and seven cellular proteins were only present in hypoxia and

1177 2408 were common to the 3 experimental conditions. **B.** Seventeen secreted proteins were
1178 only present in hypoxia and 252 were common to the 3 experimental conditions.
1179
1180 **Supplementary figure 8: GO enrichment analysis for molecular function (A,B) and cellular**
1181 **component (C,D) showed a particular pattern in hypoxia for secreted proteins (A,C) but**
1182 **not for cellular (B,D) proteins. A.** The major enriched molecular function process for
1183 secreted proteins in hypoxia was structural constituents of ribosome and in normoxia
1184 catalytic and oxidoreductase activity. **B.** For cellular component, the major enriched cellular
1185 components were the ribosome, ribonucleoprotein complex and intracellular in hypoxia and
1186 mainly ribosome in normoxia. **C.** The major enriched molecular function process for cellular
1187 proteins in hypoxia were the same as normoxia: nucleotide binding, transferase activity and
1188 catalytic activity. **D.** For cellular component, the major enriched cellular component for both
1189 hypoxia and normoxia were cytoplasm, ribosome, ribonucleoprotein complex and
1190 intracellular.
1191
1192 **Acknowledgements**

1193 We would like to acknowledge Christina A. Cuomo, Laurent Châtre, Guilhem Janbon, Jean-
1194 Yves Coppée, Pierre Rocheteau, Pierre Henri Commere, Christine Schmitt, Olivier Gorgette,
1195 Jacomine Krijnse-Locker, Caroline Proux for their comments on this work and help at
1196 different steps of the study.

1197 **References**

1198 1. Postgate JR. 1969. Chapter XVIII Viable counts and Viability, p. 611–628. *In* Methods in
1199 Microbiology. Academic Press.
1200 2. Kaprelyants AS, Mukamolova GV, Kell DB. 1994. Estimation of dormant *Micrococcus luteus*
1201 cells by penicillin lysis and by resuscitation in cell-free spent culture medium at high dilution.
1202 FEMS Microbiol Lett 115:347.
1203 3. Emerson JB, Adams RI, Román CMB, Brooks B, Coil DA, Dahlhausen K, Ganz HH, Hartmann EM,
1204 Hsu T, Justice NB, Paulino-Lima IG, Luongo JC, Lymperopoulou DS, Gomez-Silvan C, Rothschild-
1205 Mancinelli B, Balk M, Huttenhower C, Nocker A, Vaishampayan P, Rothschild LJ. 2017.
1206 Schrödinger's microbes: Tools for distinguishing the living from the dead in microbial
1207 ecosystems. Microbiome 5:86.
1208 4. Roszak DB, Colwell RR. 1987. Survival strategies of bacteria in the natural environment.
1209 Microbiol Rev 51:365–379.
1210 5. Nyström T. 2003. Nonculturable bacteria: programmed survival forms or cells at death's door?
1211 BioEssays News Rev Mol Cell Dev Biol 25:204–211.
1212 6. Oliver JD. 2010. Recent findings on the viable but nonculturable state in pathogenic bacteria.
1213 FEMS Microbiol Rev 34:415–425.
1214 7. Ayrapetyan M, Williams TC, Baxter R, Oliver JD. 2015. Viable but Nonculturable and Persister
1215 Cells Coexist Stochastically and Are Induced by Human Serum. Infect Immun 83:4194–4203.
1216 8. Li L, Mendis N, Trigui H, Oliver JD, Faucher SP. 2014. The importance of the viable but non-
1217 culturable state in human bacterial pathogens. Front Microbiol 5:258.
1218 9. Divol B, Lonvaud-Funel A. 2005. Evidence for viable but nonculturable yeasts in botrytis-
1219 affected wine. J Appl Microbiol 99:85–93.
1220 10. Salma M, Rousseaux S, Grand AS-L, Divol B, Alexandre H. 2013. Characterization of the Viable
1221 but Nonculturable (VBNC) State in *Saccharomyces cerevisiae*. PloS One 8:e77600.
1222 11. Serpaggi V, Remize F, Recorbet G, Gaudot-Dumas E, Sequeira-Le Grand A, Alexandre H. 2012.
1223 Characterization of the "viable but nonculturable" (VBNC) state in the wine spoilage yeast
1224 Brettanomyces. Food Microbiol 30:438–447.
1225 12. Brunet K, Alanio A, Lortholary O, Rammaert B. 2018. Reactivation of dormant/latent fungal
1226 infection. J Infect 77:463–468.
1227 13. Lewenza S, Abboud J, Poon K, Kobryn M, Humplik I, Bell JR, Mardan L, Reckseidler-Zenteno S.
1228 2018. Pseudomonas aeruginosa displays a dormancy phenotype during long-term survival in
1229 water. PloS One 13:e0198384.
1230 14. Helaine S, Cheverton AM, Watson KG, Faure LM, Matthews SA, Holden DW. 2014.
1231 Internalization of *Salmonella* by macrophages induces formation of nonreplicating persisters.
1232 Science 343:204–208.
1233 15. Markus MB. 2018. Biological concepts in recurrent *Plasmodium vivax* malaria. Parasitology
1234 145:1765–1771.
1235 16. Rittershaus ESC, Baek S-H, Sassetti CM. 2013. The normalcy of dormancy: common themes in
1236 microbial quiescence. Cell Host Microbe 13:643–651.
1237 17. Garcia-Hermoso D, Janbon G, Dromer F. 1999. Epidemiological evidence for dormant
1238 Cryptococcus neoformans infection. Cryptococcus Neoformans 37:3204–3209.
1239 18. Dromer F, Ronin O, Dupont B. 1992. Isolation of *Cryptococcus neoformans* var. *gattii* from an
1240 Asian patient in France: evidence for dormant infection in healthy subjects. J Med Vet Mycol
1241 Bi-Mon Publ Int Soc Hum Anim Mycol 30:395–397.
1242 19. Kwon-Chung KJ, Bennett JE. 1992. Medical mycology. Philadelphia: Lea & Febiger.
1243 20. Rajasingham R, Smith RM, Park BJ, Jarvis JN, Govender NP, Chiller TM, Denning DW, Loyse A,
1244 Boulware DR. 2017. Global burden of disease of HIV-associated cryptococcal meningitis: an
1245 updated analysis. Lancet Infect Dis 17:873.

1246 21. Baker RD. 1976. The primary pulmonary lymph node complex of crytptococcosis. Am J Clin
1247 Pathol 65:83–92.
1248 22. Goldman D, Lee SC, Casadevall A. 1994. Pathogenesis of pulmonary Cryptococcus neoformans
1249 infection in the rat. Infect Immun 62:4755–4761.
1250 23. Alanio A, Vernel-Pauillac F, Sturny-Leclère A, Dromer F. 2015. Cryptococcus neoformans host
1251 adaptation: toward biological evidence of dormancy. mBio 6:e02580-14.
1252 24. Rocheteau P, Vinet M, Chretien F. 2015. Dormancy and quiescence of skeletal muscle stem
1253 cells. Results Probl Cell Differ 56:215–235.
1254 25. Albuquerque P, Nicola AM, Nieves E, Paes HC, Williamson PR, Silva-Pereira I, Casadevall A.
1255 2013. Quorum sensing-mediated, cell density-dependent regulation of growth and virulence in
1256 *Cryptococcus neoformans*. mBio 5:e00986-13.
1257 26. Baker RD, Haugen RK. 1955. Tissue Changes and Tissue Diagnosis in Cryptococcosis: A Study of
1258 26 Cases. Am J Clin Pathol 25:14.
1259 27. Haugen RK, Baker RD. 1954. The Pulmonary Lesions in Cryptococcosis with Special References
1260 to Subpleural Nodules. Am J Clin Pathol 24:1381.
1261 28. Idnurm A, Bahn Y-S, Nielsen K, Lin X, Fraser JA, Heitman J. 2005. Deciphering the model
1262 pathogenic fungus *Cryptococcus neoformans*. Nat Rev Microbiol 3:753–764.
1263 29. De Virgilio C. 2012. The essence of yeast quiescence. FEMS Microbiol Rev 36:306–339.
1264 30. Grahl N, Shepardson KM, Chung D, Cramer RA. 2012. Hypoxia and fungal pathogenesis: to air
1265 or not to air? Eukaryot Cell 11:560–570.
1266 31. Wayne LG, Hayes LG. 1996. An in vitro model for sequential study of shiftdown of
1267 *Mycobacterium tuberculosis* through two stages of nonreplicating persistence. Infect Immun
1268 64:2062–2069.
1269 32. Semighini CP, Averette AF, Perfect JR, Heitman J. 2011. Deletion of *Cryptococcus neoformans*
1270 AIF ortholog promotes chromosome aneuploidy and fluconazole-resistance in a metacaspase-
1271 independent manner. PLoS Pathog 7:e1002364.
1272 33. Day AP, Oliver JD. 2004. Changes in membrane fatty acid composition during entry of *Vibrio*
1273 *vulnificus* into the viable but nonculturable state. J Microbiol Seoul Korea 42:69–73.
1274 34. Latil M, Rocheteau P, Châtre L, Sanulli S, Mémet S, Ricchetti M, Tajbakhsh S, Chrétien F. 2012.
1275 Skeletal muscle stem cells adopt a dormant cell state post mortem and retain regenerative
1276 capacity. Nat Commun 3:903.
1277 35. DuBois JC, Pasula R, Dade JE, Smulian AG. 2016. Yeast Transcriptome and In Vivo Hypoxia
1278 Detection Reveals *Histoplasma capsulatum* Response to Low Oxygen Tension. Med Mycol
1279 54:40–58.
1280 36. Qualls JE, Murray PJ. 2016. Immunometabolism within the tuberculosis granuloma: amino
1281 acids, hypoxia, and cellular respiration. Semin Immunopathol 38:139–152.
1282 37. Sershen CL, Plimpton SJ, May EE. 2016. Oxygen Modulates the Effectiveness of Granuloma
1283 Mediated Host Response to *Mycobacterium tuberculosis*: A Multiscale Computational Biology
1284 Approach. Front Cell Infect Microbiol 6:6.
1285 38. Lane SW, Williams DA, Watt FM. 2014. Modulating the stem cell niche for tissue regeneration.
1286 Nat Biotechnol 32:795–803.
1287 39. Mathieu J, Zhou W, Xing Y, Sperber H, Ferreccio A, Agoston Z, Kuppusamy KT, Moon RT,
1288 Ruohola-Baker H. 2014. Hypoxia-inducible factors have distinct and stage-specific roles during
1289 reprogramming of human cells to pluripotency. Cell Stem Cell 14:592–605.
1290 40. Dong Z, Wang JZ, Yu F, Venkatachalam MA. 2003. Apoptosis-Resistance of Hypoxic Cells:
1291 Multiple Factors Involved and a Role for IAP-2. Am J Pathol 163:663–671.
1292 41. Wu J, Parungo C, Wu G, Kang PM, Laham RJ, Sellke FW, Simons M, Li J. 2004. PR39 inhibits
1293 apoptosis in hypoxic endothelial cells: role of inhibitor apoptosis protein-2. Circulation
1294 109:1660–1667.
1295 42. Graeber TG, Osmanian C, Jacks T, Housman DE, Koch CJ, Lowe SW, Giaccia AJ. 1996. Hypoxia-
1296 mediated selection of cells with diminished apoptotic potential in solid tumours. Nature
1297 379:88–91.

1298 43. Arana I, Orruño M, Pérez-Pascual D, Seco C, Muela A, Barcina I. 2007. Inability of *Escherichia*
1299 *coli* to resuscitate from the viable but nonculturable state. FEMS Microbiol Ecol 62:1–11.
1300 44. Li L, Mendis N, Trigui H, Oliver JD, Faucher SP. 2014. The importance of the viable but non-
1301 culturable state in human bacterial pathogens. Front Microbiol 5:258.
1302 45. Spry C, Kirk K, Saliba KJ. 2008. Coenzyme A biosynthesis: an antimicrobial drug target. FEMS
1303 Microbiol Rev 32:56–106.
1304 46. Liew KL, Jee JM, Yap I, Yong PVC. 2016. In Vitro Analysis of Metabolites Secreted during
1305 Infection of Lung Epithelial Cells by *Cryptococcus neoformans*. PloS One 11:e0153356.
1306 47. Calcott PH, Postgate JR. 1972. On substrate-accelerated death in *Klebsiella aerogenes*. J Gen
1307 Microbiol 70:115–122.
1308 48. Mukamolova GV, Kaprelyants AS, Kell DB, Young M. 2003. Adoption of the transiently non-
1309 culturable state — a bacterial survival strategy?
1310 49. Nofal M, Zhang K, Han S, Rabinowitz JD. 2017. mTOR Inhibition Restores Amino Acid Balance in
1311 Cells Dependent on Catabolism of Extracellular Protein. Mol Cell 67:936-946.e5.
1312 50. Oblinger JL, Koburger JA. 1975. Understanding and Teaching the Most Probable Number
1313 Technique. J Milk Food Technol 38:540–545.
1314 51. Pinto D, Santos MA, Chambel L. 2013. Thirty years of viable but nonculturable state research:
1315 unsolved molecular mechanisms. Crit Rev Microbiol 41:61–76.
1316 52. Blackburn CW, McCarthy JD. 2000. Modifications to methods for the enumeration and
1317 detection of injured Escherichia coli O157:H7 in foods. Int J Food Microbiol 55:285–290.
1318 53. Steenbergen JN, Shuman HA, Casadevall A. 2001. *Cryptococcus neoformans* interactions with
1319 amoebae suggest an explanation for its virulence and intracellular pathogenic strategy in
1320 macrophages. Proc Natl Acad Sci U S A 98:15245–15250.
1321 54. García MT, Jones S, Pelaz C, Millar RD, Abu Kwaik Y. 2007. *Acanthamoeba polyphaga*
1322 resuscitates viable non-culturable *Legionella pneumophila* after disinfection. Environ Microbiol
1323 9:1267–1277.
1324 55. Steinert M, Emödy L, Amann R, Hacker J. 1997. Resuscitation of viable but nonculturable
1325 *Legionella pneumophila* Philadelphia JR32 by *Acanthamoeba castellanii*. Appl Environ
1326 Microbiol 63:2047–2053.
1327 56. Schumann R, Rieling T, Görs S, Hammer A, Selig U, Schiewer U. 2003. Viability of bacteria from
1328 different aquatic habitats. I. Environmental conditions and productivity. Aquat Microb Ecol
1329 32:121–135.
1330 57. Sebastià J, Cristòfol R, Martín M, Rodríguez-Farré E, Sanfeliu C. 2003. Evaluation of fluorescent
1331 dyes for measuring intracellular glutathione content in primary cultures of human neurons and
1332 neuroblastoma SH-SY5Y. Cytometry A 51A:16–25.
1333 58. DeRisi JL, Iyer VR, Brown PO. 1997. Exploring the metabolic and genetic control of gene
1334 expression on a genomic scale. Science 278:680–686.
1335 59. Boucherie H. 1985. Protein synthesis during transition and stationary phases under glucose
1336 limitation in *Saccharomyces cerevisiae*. J Bacteriol 161:385–392.
1337 60. Fuge EK, Braun EL, Werner-Washburne M. 1994. Protein synthesis in long-term stationary-
1338 phase cultures of *Saccharomyces cerevisiae*. J Bacteriol 176:5802–5813.
1339 61. Ju Q, Warner JR. 1994. Ribosome synthesis during the growth cycle of *Saccharomyces*
1340 *cerevisiae*. Yeast Chichester Engl 10:151–157.
1341 62. Lee J, Giordano S, Zhang J. 2012. Autophagy, mitochondria and oxidative stress: cross-talk and
1342 redox signalling. Biochem J 441:523–540.
1343 63. Rodrigues ML, Nakayasu ES, Oliveira DL, Nimrichter L, Nosanchuk JD, Almeida IC, Casadevall A.
1344 2008. Extracellular vesicles produced by *Cryptococcus neoformans* contain protein
1345 components associated with virulence. Eukaryot Cell 7:58–67.
1346 64. Geddes JMH, Croll D, Caza M, Stoynov N, Foster LJ, Kronstad JW. 2015. Secretome profiling of
1347 *Cryptococcus neoformans* reveals regulation of a subset of virulence-associated proteins and
1348 potential biomarkers by protein kinase A. BMC Microbiol 15:206.

1349 65. Lev S, Crossett B, Cha SY, Desmarini D, Li C, Chayakulkeeree M, Wilson CF, Williamson PR,
1350 Sorrell TC, Djordjevic JT. 2014. Identification of Aph1, a phosphate-regulated, secreted, and
1351 vacuolar acid phosphatase in *Cryptococcus neoformans*. mBio 5:e01649-14.
1352 66. Eisenman HC, Frases S, Nicola AM, Rodrigues ML, Casadevall A. 2009. Vesicle-associated
1353 melanization in *Cryptococcus neoformans*. Microbiol Read Engl 155:3860–3867.
1354 67. Rodrigues ML, Nakayasu ES, Oliveira DL, Nimrichter L, Nosanchuk JD, Almeida IC, Casadevall A.
1355 2007. Extracellular vesicles produced by *Cryptococcus neoformans* contain protein
1356 components associated with virulence. Eukaryot Cell 7:58–67.
1357 68. Rodrigues ML, Djordjevic JT. 2012. Unravelling secretion in *Cryptococcus neoformans*: more
1358 than one way to skin a cat. Mycopathologia 173:407–418.
1359 69. de Gassart A, Geminard C, Fevrier B, Raposo G, Vidal M. 2003. Lipid raft-associated protein
1360 sorting in exosomes. Blood 102:4336–4344.
1361 70. Homer CM, Summers DK, Goranov AI, Clarke SC, Wiesner DL, Diedrich JK, Moresco JJ, Toffaletti
1362 D, Upadhya R, Caradonna I, Petnic S, Pessino V, Cuomo CA, Lodge JK, Perfect J, Yates JR,
1363 Nielsen K, Craik CS, Madhani HD. 2016. Intracellular Action of a Secreted Peptide Required for
1364 Fungal Virulence. Cell Host Microbe 19:849–864.
1365 71. Lee H, Chang YC, Nardone G, Kwon-Chung KJ. 2007. TUP1 disruption in Cryptococcus
1366 neoformans uncovers a peptide-mediated density-dependent growth phenomenon that
1367 mimics quorum sensing. Mol Microbiol 64:591.
1368 72. Lee H, Chang YC, Varma A, Kwon-Chung KJ. 2009. Regulatory diversity of TUP1 in *Cryptococcus*
1369 *neoformans*. Eukaryot Cell 8:1901–1908.
1370 73. Selvan LDN, Kaviyil JE, Nirujogi RS, Muthusamy B, Puttamallesh VN, Subbannayya T, Syed N,
1371 Radhakrishnan A, Kelkar DS, Ahmad S, Pinto SM, Kumar P, Madugundu AK, Nair B, Chatterjee
1372 A, Pandey A, Ravikumar R, Gowda H, Prasad TSK. 2014. Proteogenomic analysis of pathogenic
1373 yeast *Cryptococcus neoformans* using high resolution mass spectrometry. Clin Proteomics 11:5.
1374 74. Selvan LDN, Sreenivasamurthy SK, Kumar S, Yelamanchi SD, Madugundu AK, Anil AK, Renuse S,
1375 Nair BG, Gowda H, Mathur PP, Satishchandra P, Shankar SK, Mahadevan A, Keshava Prasad TS.
1376 2015. Characterization of host response to *Cryptococcus neoformans* through quantitative
1377 proteomic analysis of cryptococcal meningitis co-infected with HIV. Mol Biosyst 11:2529–2540.
1378 75. Huang M, Hebert AS, Coon JJ, Hull CM. 2015. Protein Composition of Infectious Spores Reveals
1379 Novel Sexual Development and Germination Factors in *Cryptococcus*. PLoS Genet
1380 11:e1005490.
1381 76. Jamieson DJ. 1998. Oxidative stress responses of the yeast *Saccharomyces cerevisiae*. Yeast
1382 Chichester Engl 14:1511–1527.
1383 77. De Virgilio C, Loewith R. 2006. The TOR signalling network from yeast to man. Int J Biochem
1384 Cell Biol 38:1476–1481.
1385 78. Rohde J, Heitman J, Cardenas ME. 2001. The TOR kinases link nutrient sensing to cell growth. J
1386 Biol Chem 276:9583–9586.
1387 79. García-Rodas R, Cordero RJB, Trevijano-Contador N, Janbon G, Moyrand F, Casadevall A,
1388 Zaragoza O. 2014. Capsule growth in *Cryptococcus neoformans* is coordinated with cell cycle
1389 progression. mBio 5:e00945-14.
1390 80. Martinez DL, Tsuchiya Y, Gout I. 2014. Coenzyme A biosynthetic machinery in mammalian cells.
1391 Biochem Soc Trans 42:1112–1117.
1392 81. Srinivasan B, Sibon OCM. 2014. Coenzyme A, more than "just" a metabolic cofactor. Biochem
1393 Soc Trans 42:1075–1079.
1394 82. Kretschmer M, Wang J, Kronstad JW. 2012. Peroxisomal and mitochondrial β-oxidation
1395 pathways influence the virulence of the pathogenic fungus *Cryptococcus neoformans*. Eukaryot
1396 Cell 11:1042–1054.
1397 83. Itoh T, Waki H, Kaneko H. 1975. Changes of Lipid Composition with Growth Phase of
1398 *Cryptococcus neoformans*. Agric Biol Chem 39:2365–2371.
1399 84. Lorenz MC, Bender JA, Fink GR. 2004. Transcriptional response of *Candida albicans* upon
1400 internalization by macrophages. Eukaryot Cell 3:1076–1087.

1401 85. Hu G, Cheng P-Y, Sham A, Perfect JR, Kronstad JW. 2008. Metabolic adaptation in *Cryptococcus*
1402 *neoformans* during early murine pulmonary infection. Mol Microbiol 69:1456–1475.
1403 86. da S Derengowski L, Paes HC, Albuquerque P, Tavares AHFP, Fernandes L, Silva-Pereira I,
1404 Casadevall A. 2013. The transcriptional response of *Cryptococcus neoformans* to ingestion by
1405 *Acanthamoeba castellanii* and macrophages provides insights into the evolutionary adaptation
1406 to the mammalian host. Eukaryot Cell 12:761–774.
1407 87. Hommel B, Mukaremera L, Cordero RJB, Coelho C, Desjardins CA, Sturny-Leclère A, Janbon G,
1408 Perfect JR, Fraser JA, Casadevall A, Cuomo CA, Dromer F, Nielsen K, Alanio A. 2018. Titan cells
1409 formation in *Cryptococcus neoformans* is finely tuned by environmental conditions and
1410 modulated by positive and negative genetic regulators. PLoS Pathog 14:e1006982.
1411 88. Ferreira GF, de Matos Baltazar L, Santos JRA, Monteiro AS, de Oliveira Fraga LA, Resende-
1412 Stoianoff MA, Santos DA. 2013. The role of oxidative and nitrosative bursts caused by azoles
1413 and amphotericin B against the fungal pathogen *Cryptococcus gattii*. J Antimicrob Chemother
1414 68:1801–1811.
1415 89. Kahm M, Hasenbrink G, Lichtenberg-Fraté H, Ludwig J, Kschischo M. 2010. grofit: Fitting
1416 Biological Growth Curves withR. J Stat Softw 33.
1417 90. Alanio A, Desnos-Ollivier M, Dromer F. 2011. Dynamics of *Cryptococcus neoformans*-
1418 macrophage interactions reveal that fungal background influences outcome during
1419 cryptococcal meningoencephalitis in humans. mBio 2:e00158-11.
1420 91. Casadevall A, DeShaw M, Fan M, Dromer F, Kozel TR, Pirofski L a. 1994. Molecular and idiotypic
1421 analysis of antibodies to *Cryptococcus neoformans* glucuronoxylomannan. Infect Immun
1422 62:3864–3872.
1423 92. Nielsen K, Cox GM, Litvintseva AP, Mylonakis E, Malliaris SD, Benjamin DK, Giles SS, Mitchell
1424 TG, Casadevall A, Perfect JR, Heitman J. 2005. *Cryptococcus neoformans* {alpha} strains
1425 preferentially disseminate to the central nervous system during coinfection. Infect Immun
1426 73:4922–4933.
1427 93. Bochner BR, Gadzinski P, Panomitros E. 2001. Phenotype microarrays for high-throughput
1428 phenotypic testing and assay of gene function. Genome Res 11:1246–1255.
1429 94. Moyrand F, Lafontaine I, Fontaine T, Janbon G. 2008. UGE1 and UGE2 regulate the UDP-
1430 glucose/UDP-galactose equilibrium in *Cryptococcus neoformans*. Eukaryot Cell 7:2069–2077.
1431 95. Vandesompele J, De Preter K, Pattyn F, Poppe B, Van Roy N, De Paepe A, Speleman F. 2002.
1432 Accurate normalization of real-time quantitative RT-PCR data by geometric averaging of
1433 multiple internal control genes. Genome Biol 3:RESEARCH0034.
1434 96. Pfaffl MW. 2001. A new mathematical model for relative quantification in real-time RT–PCR.
1435 Nucleic Acids Res 29:e45.
1436 97. Wu X, Xiong E, Wang W, Scali M, Cresti M. 2014. Universal sample preparation method
1437 integrating trichloroacetic acid/acetone precipitation with phenol extraction for crop
1438 proteomic analysis. Nat Protoc 9:362–374.
1439 98. Cox J, Neuhauser N, Michalski A, Scheltema RA, Olsen JV, Mann M. 2011. Andromeda: a
1440 peptide search engine integrated into the MaxQuant environment. J Proteome Res 10:1794–
1441 1805.
1442 99. Cox J, Mann M. 2008. MaxQuant enables high peptide identification rates, individualized
1443 p.p.b.-range mass accuracies and proteome-wide protein quantification. Nat Biotechnol
1444 26:1367–1372.
1445 100. Tyanova S, Temu T, Cox J. 2016. The MaxQuant computational platform for mass
1446 spectrometry-based shotgun proteomics. Nat Protoc 11:2301–2319.
1447 101. Cox J, Hein MY, Luber CA, Paron I, Nagaraj N, Mann M. 2014. Accurate proteome-wide label-
1448 free quantification by delayed normalization and maximal peptide ratio extraction, termed
1449 MaxLFQ. Mol Cell Proteomics MCP 13:2513–2526.
1450 102. Bø TH, Dysvik B, Jonassen I. 2004. LSimpute: accurate estimation of missing values in
1451 microarray data with least squares methods. Nucleic Acids Res 32:e34.

1452 103. Gower JC. 1966. Some distance properties of latent root and vector methods used in
1453 multivariate analysis. Biometrika 325–38.
1454 104. Ritchie ME, Phipson B, Wu, Hu Y, Law CW, Shi W, Smyth GK. 2015. limma powers differential
1455 expression analyses for RNA-sequencing and microarray studies. Nucleic Acids Res 43:e47.
1456 105. Benjamini Y, Hochberg Y. 1995. Controlling the False Discovery Rate: A Practical and Powerful
1457 Approach to Multiple Testing. J R Stat Soc Ser B Methodol 57:289–300.
1458 106. Priebe S, Kreisel C, Horn F, Guthke R, Linde J. 2014. FungiFun2: a comprehensive online
1459 resource for systematic analysis of gene lists from fungal species. Bioinforma Oxf Engl 31:445–
1460 446.
1461 107. Bardou P, Mariette J, Escudié F, Djemiel C, Klopp C. 2014. jvenn: an interactive Venn diagram
1462 viewer. BMC Bioinformatics 15.
1463 108. Szklarczyk D, Franceschini A, Wyder S, Forslund K, Heller D, Huerta-Cepas J, Simonovic M, Roth
1464 A, Santos A, Tsafou KP, Kuhn M, Bork P, Jensen LJ, von Mering C. 2014. STRING v10: protein-
1465 protein interaction networks, integrated over the tree of life. Nucleic Acids Res 43:D447-52.
1466 109. Martin M. 2011. Cutadapt removes adapter sequences from high-throughput sequencing
1467 reads. EMBnet.journal 17:10–12.
1468 110. Dobin A, Davis CA, Schlesinger F, Drenkow J, Zaleski C, Jha S, Batut P, Chaisson M, Gingeras TR.
1469 2013. STAR: ultrafast universal RNA-seq aligner. Bioinformatics 29:15–21.
1470 111. Liao Y, Smyth GK, Shi W. 2014. featureCounts: an efficient general purpose program for
1471 assigning sequence reads to genomic features. Bioinforma Oxf Engl 30:923–930.
1472 112. Ewels P, Magnusson M, Lundin S, Käller M. 2016. MultiQC: summarize analysis results for
1473 multiple tools and samples in a single report. Bioinformatics 32:3047–3048.
1474 113. Love MI, Huber W, Anders S. 2014. Moderated estimation of fold change and dispersion for
1475 RNA-seq data with DESeq2. Genome Biol 15:550.
1476 114. Basenko EY, Pulman JA, Shanmugasundram A, Harb OS, Crouch K, Starns D, Warrenfeltz S,
1477 Aurrecoechea C, Stoeckert CJ, Kissinger JC, Roos DS, Hertz-Fowler C. 2018. FungiDB: An
1478 Integrated Bioinformatic Resource for Fungi and Oomycetes. J Fungi Basel Switz 4.
1479 115. Marchler-Bauer A, Bo Y, Han L, He J, Lanczycki CJ, Lu S, Chitsaz F, Derbyshire MK, Geer RC,
1480 Gonzales NR, Gwadz M, Hurwitz DI, Lu F, Marchler GH, Song JS, Thanki N, Wang Z, Yamashita
1481 RA, Zhang D, Zheng C, Geer LY, Bryant SH. 2017. CDD/SPARCLE: functional classification of
1482 proteins via subfamily domain architectures. Nucleic Acids Res 45:D200–D203.
1483 116. Nielsen H. 2017. Predicting Secretory Proteins with SignalP. Methods Mol Biol Clifton NJ
1484 1611:59–73.

1485

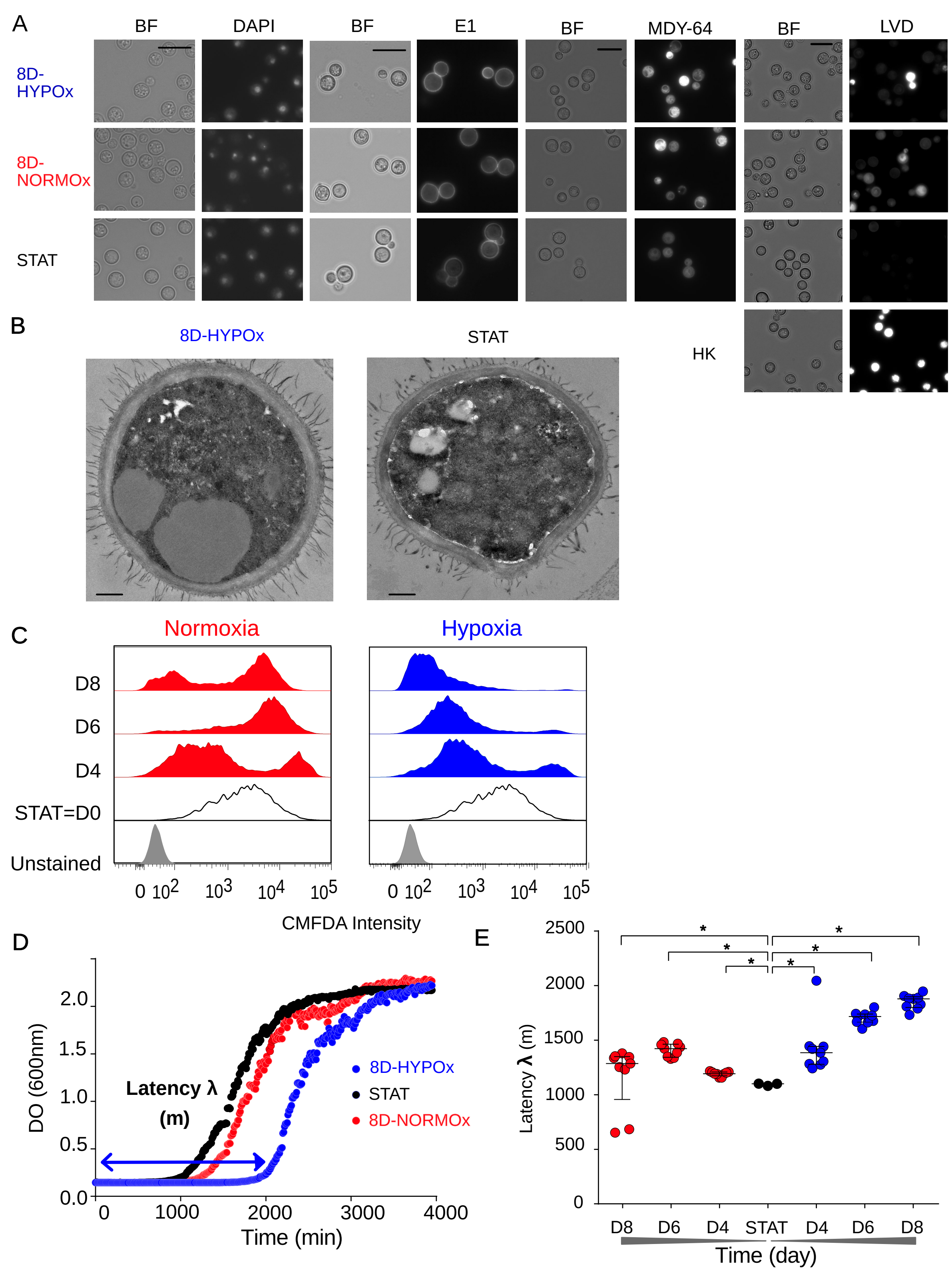
A
BF
DAPI
BF
E1
BF
MDY-64
BF
LVD
8D-HYPOx
8D-NORMOx
STAT
HK
B
8D-HYPOx
STAT
C
Normoxia
Hypoxia
D8
D6
D4
STAT=D0
Unstained
0 10^2 10^3 10^4 10^5
CMFDA Intensity
D
DO (600nm)
Latency λ (m)
8D-HYPOx
STAT
8D-NORMOx
Time (min)
E
Latency λ (m)
D8 D6 D4 STAT D4 D6 D8
Time (day)

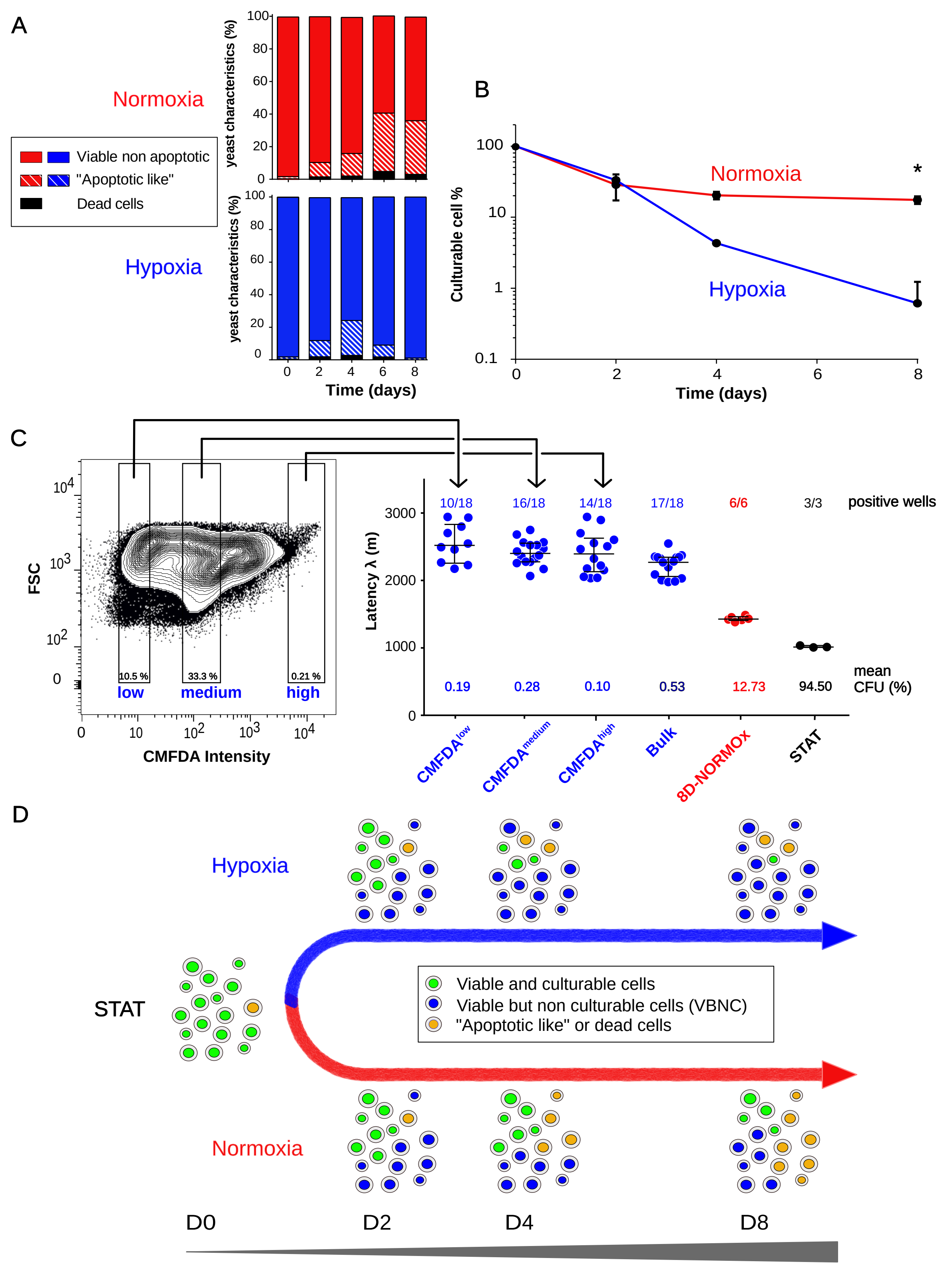
A
Normoxia
Hypoxia
Viable non apoptotic
"Apoptotic like"
Dead cells
yeast characteristics (%)
Time (days)
B
Normoxia
Hypoxia
Culturable cell %
Time (days)
C
FSC
CMFDA Intensity
10.5 %
33.3 %
0.21 %
low
medium
high
Latency λ (m)
10/18
16/18
14/18
17/18
6/6
3/3
positive wells
0.19
0.28
0.10
0.53
12.73
94.50
mean CFU (%)
CMFDA low
CMFDA medium
CMFDA high
Bulk
8D-NORMOx
STAT
D
Hypoxia
STAT
Normoxia
Viable and culturable cells
Viable but non culturable cells (VBNC)
"Apoptotic like" or dead cells
D0
D2
D4
D8

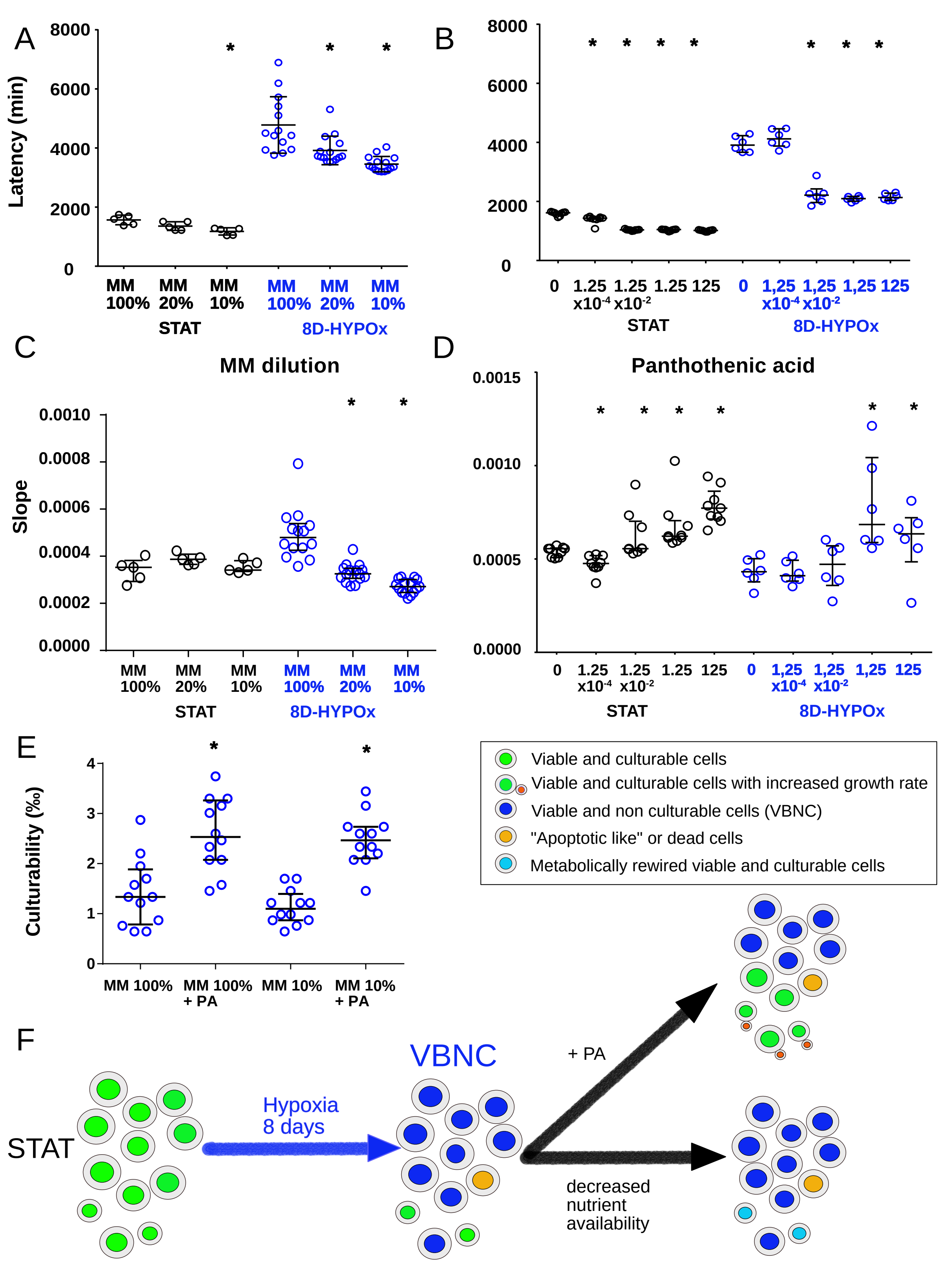
A
Latency (min)
8000
6000
4000
2000
0
MM 100%
MM 20%
MM 10%
MM 100%
MM 20%
MM 10%
STAT
8D-HYPOx
B
0
1.25 x10-4
1.25 x10-2
1.25
125
1,25 x10-4
1,25 x10-2
1,25
125
C
MM dilution
Slope
0.0010
0.0008
0.0006
0.0004
0.0002
0.0000
D
Panthothenic acid
0.0015
0.0010
0.0005
0.0000
E
Culturability (‰)
4
3
2
1
0
MM 100%
MM 100% + PA
MM 10%
MM 10% + PA
Viable and culturable cells
Viable and culturable cells with increased growth rate
Viable and non culturable cells (VBNC)
"Apoptotic like" or dead cells
Metabolically rewired viable and culturable cells
F
STAT
Hypoxia 8 days
VBNC
+ PA
decreased nutrient availability

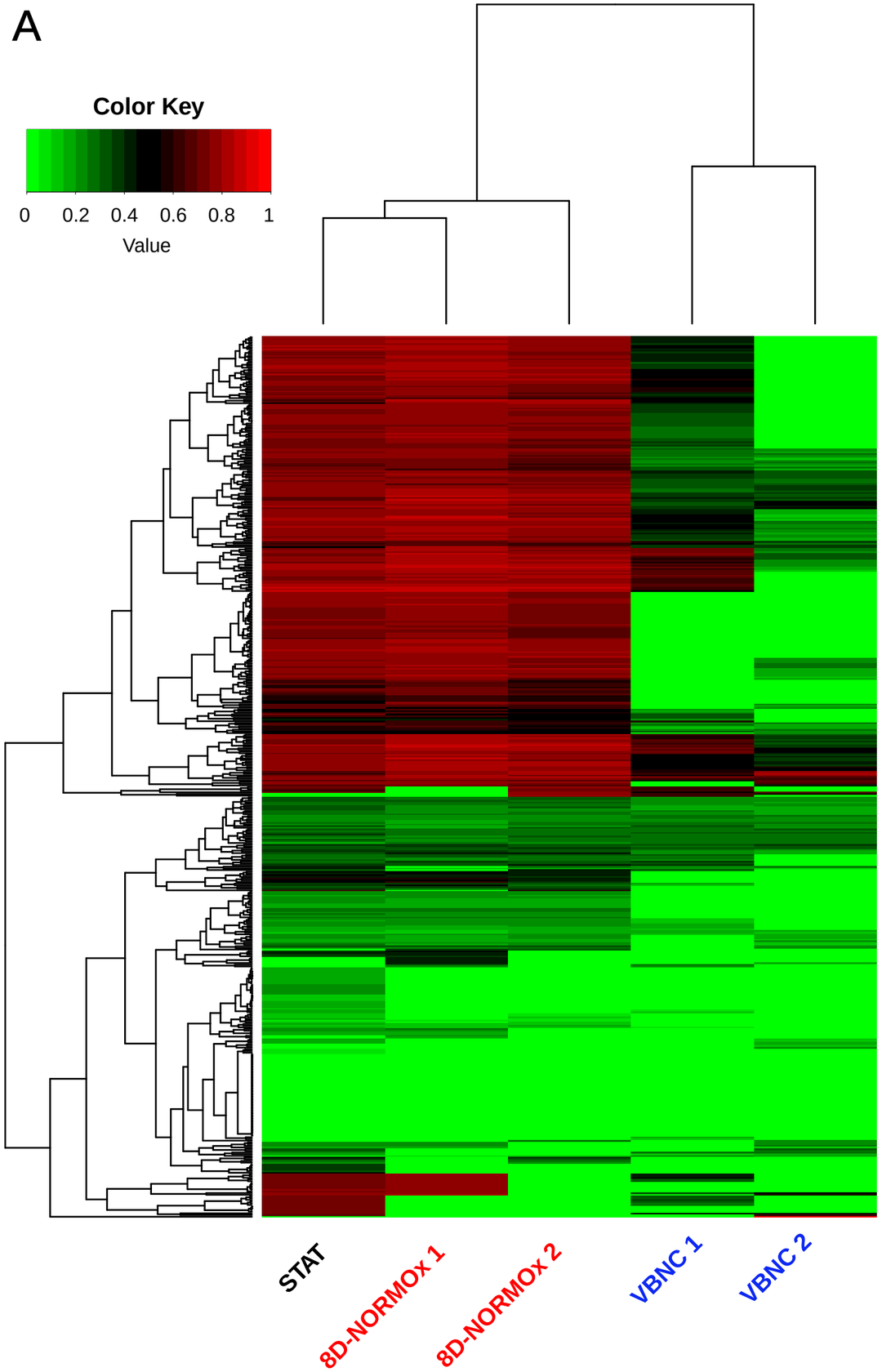
A
Color Key
0
0.2
0.4
0.6
0.8
1
Value
STAT
8D-NORMOx 1
8D-NORMOx 2
VBNC 1
VBNC 2

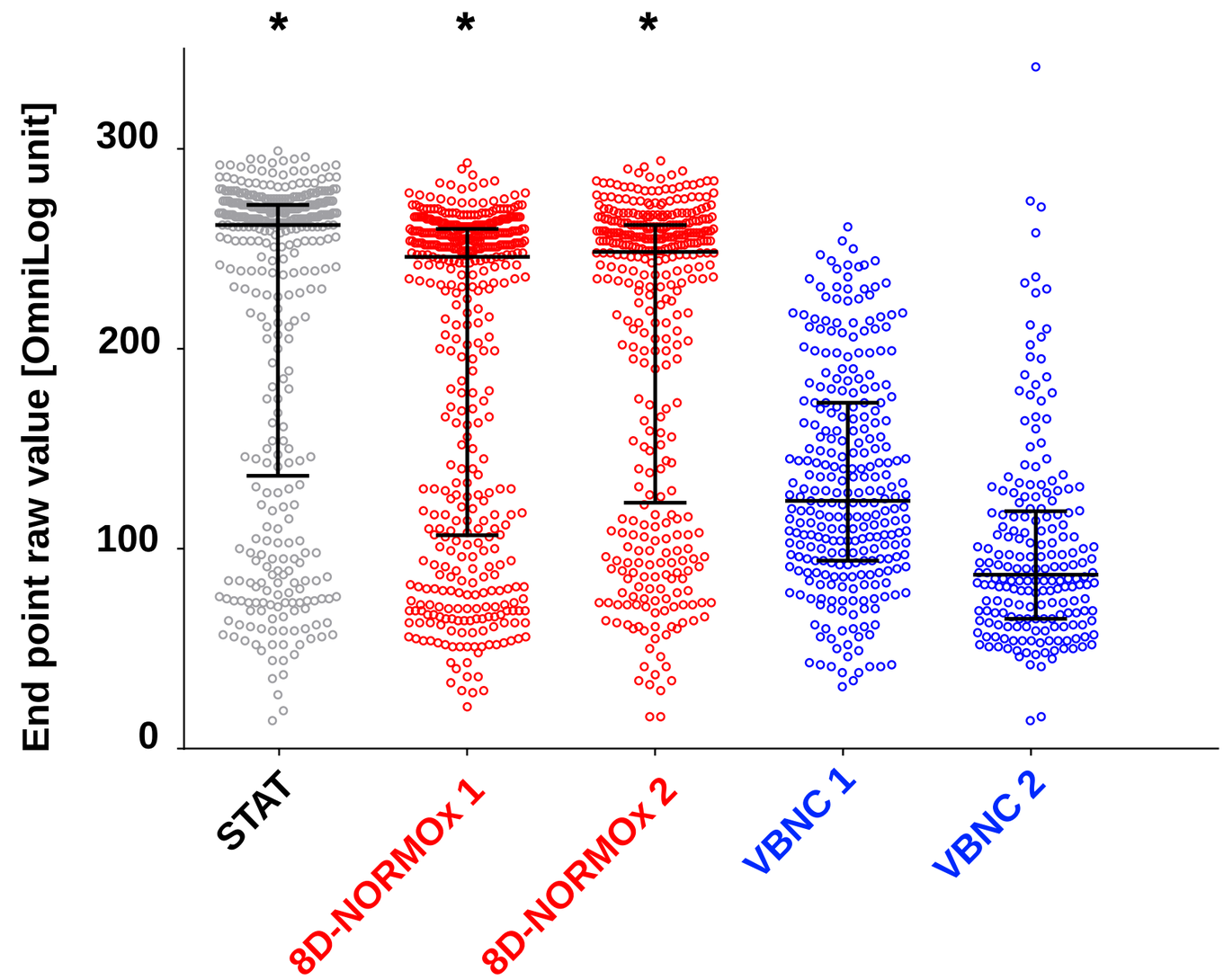
B
End point raw value [OmniLog unit]
300
200
100
0
*
*
*
STAT
8D-NORMOx 1
8D-NORMOx 2
VBNC 1
VBNC 2

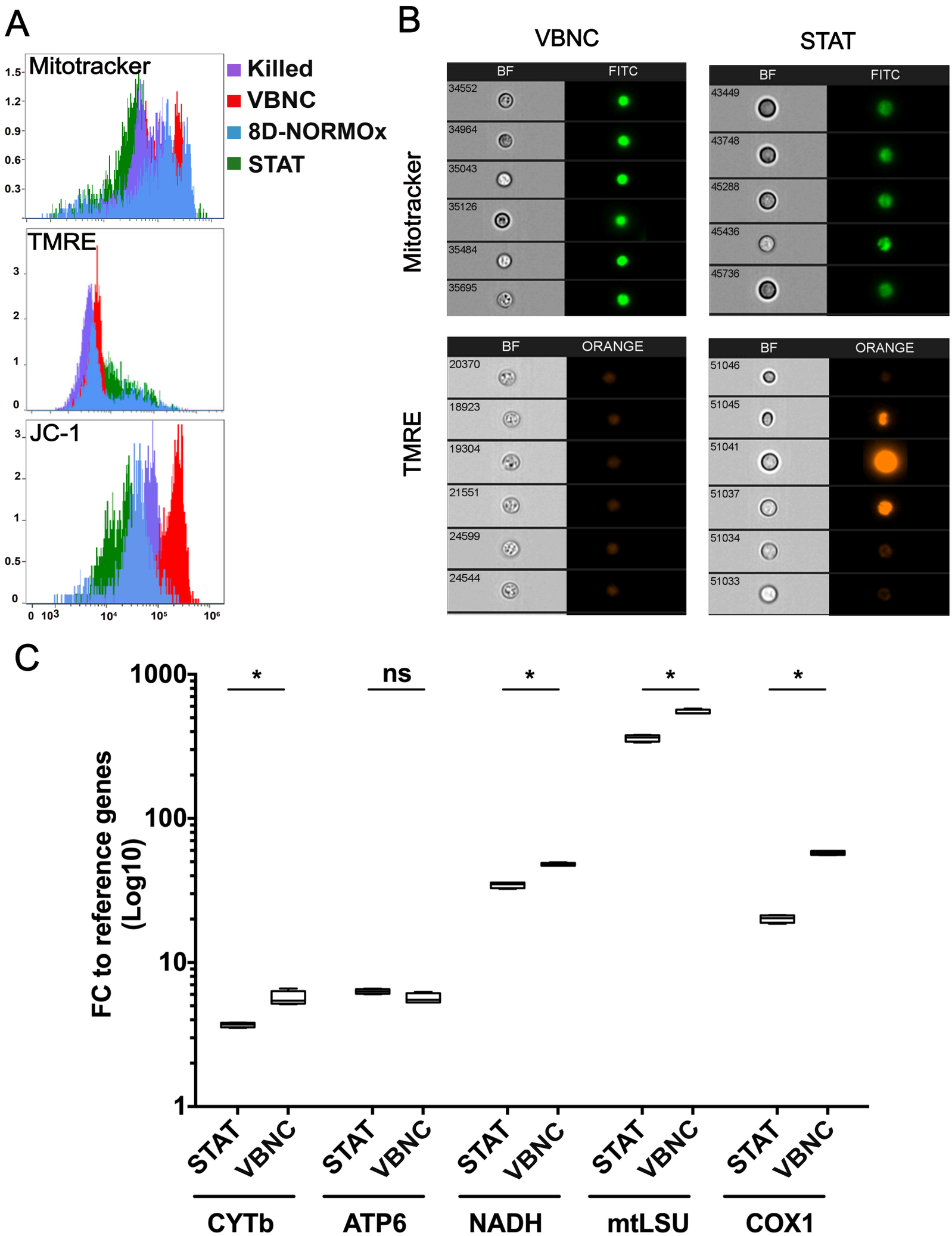
A
Mitotracker
TMRE
JC-1
Killed
VBNC
8D-NORMOx
STAT
B
VBNC
STAT
Mitotracker
TMRE
BF
FITC
ORANGE
C
FC to reference genes (Log10)
1000
100
10
1
*
ns
STAT
VBNC
CYTb
ATP6
NADH
mtLSU
COX1

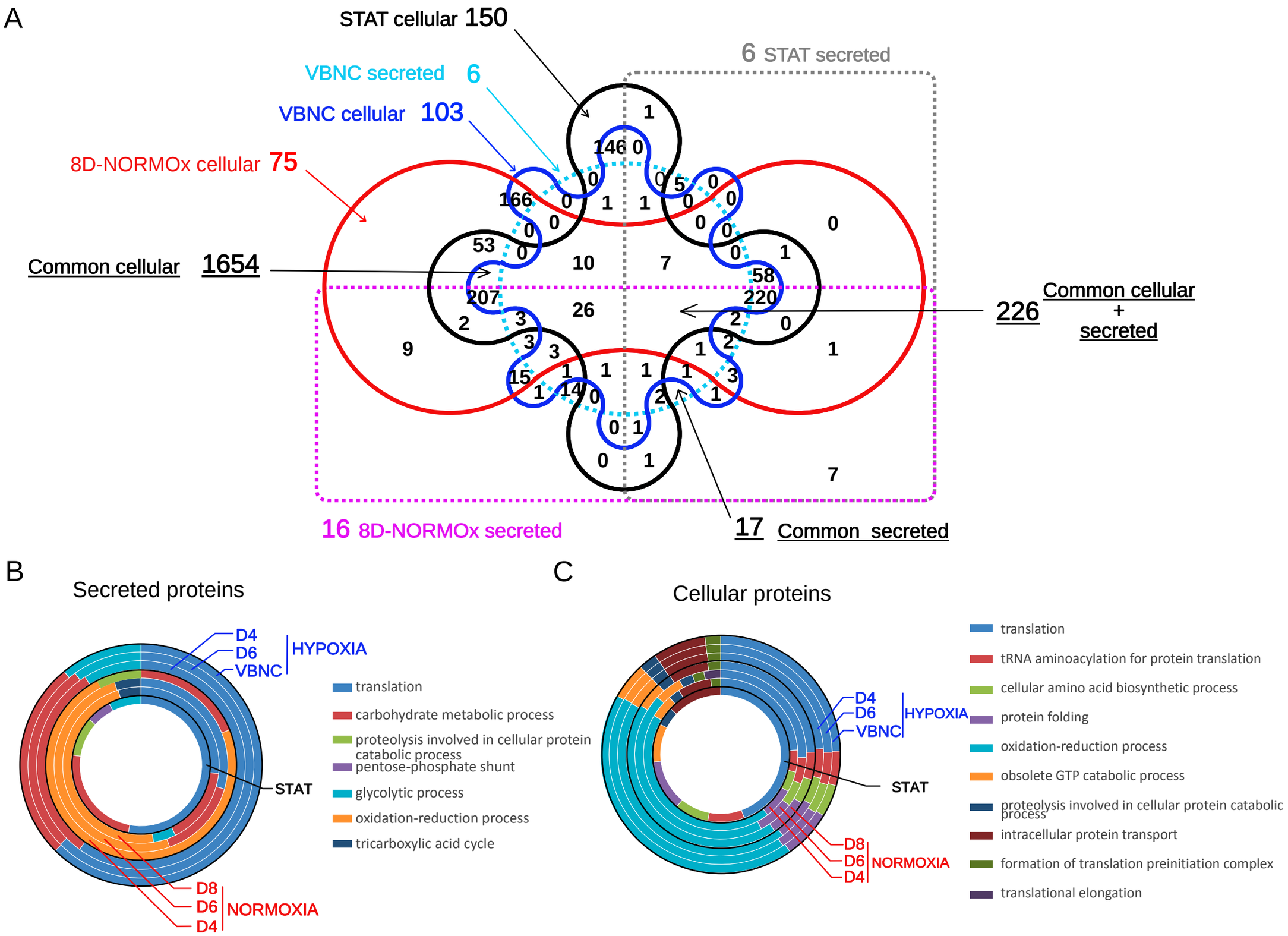
A
STAT cellular 150
6 STAT secreted
VBNC secreted 6
VBNC cellular 103
8D-NORMOx cellular 75
Common cellular 1654
226 Common cellular + secreted
16 8D-NORMOx secreted
17 Common secreted
B
Secreted proteins
D4
D6
VBNC
HYPOXIA
STAT
D8
D6
D4
NORMOXIA
translation
carbohydrate metabolic process
proteolysis involved in cellular protein catabolic process
pentose-phosphate shunt
glycolytic process
oxidation-reduction process
tricarboxylic acid cycle
C
Cellular proteins
D4
D6
VBNC
HYPOXIA
STAT
D8
D6
D4
NORMOXIA
translation
tRNA aminoacylation for protein translation
cellular amino acid biosynthetic process
protein folding
oxidation-reduction process
obsolete GTP catabolic process
proteolysis involved in cellular protein catabolic process
intracellular protein transport
formation of translation preinitiation complex
translational elongation

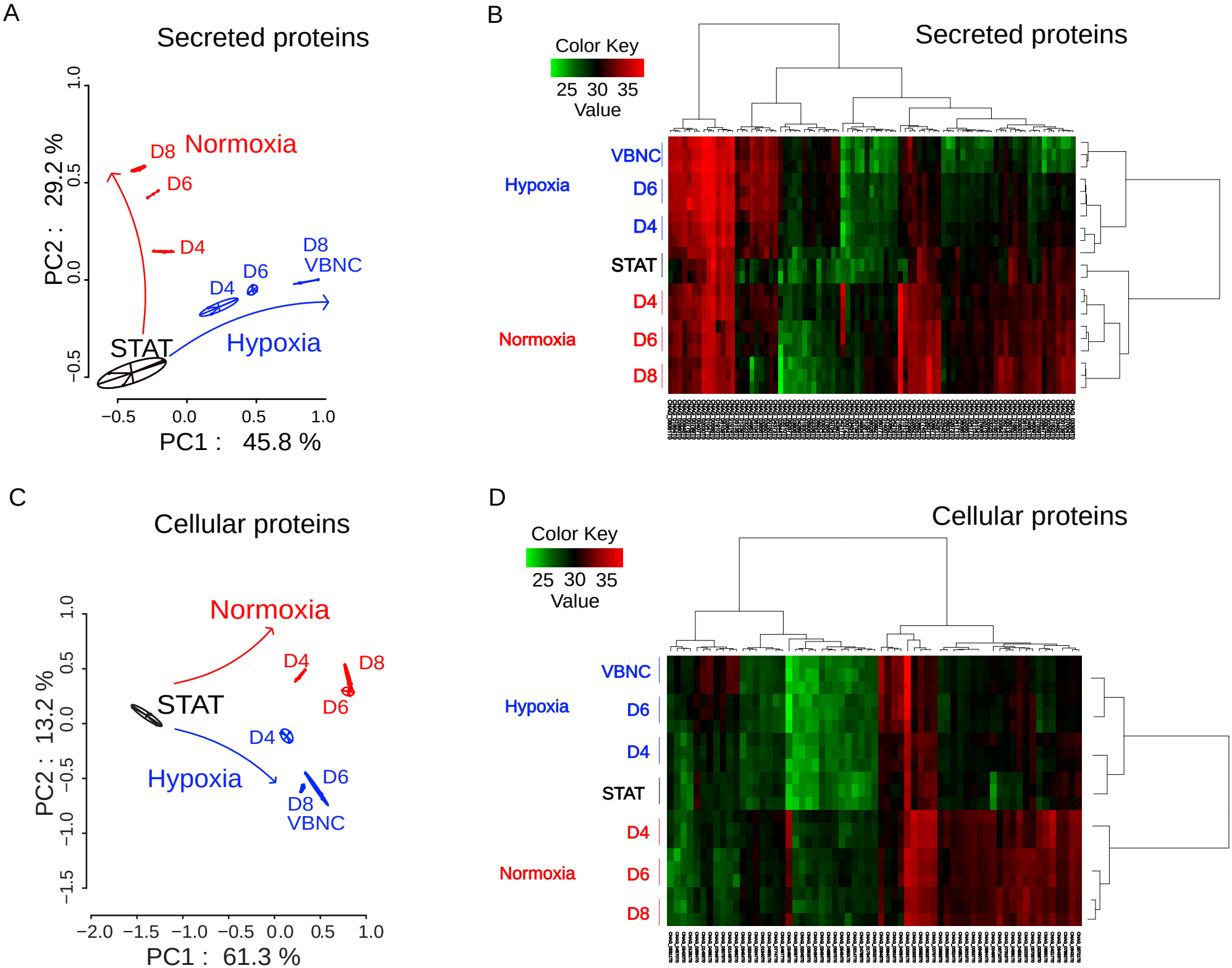
A
Secreted proteins
Normoxia
D8
D6
D4
D8
VBNC
D6
D4
STAT
Hypoxia
PC2 : 29.2 %
PC1 : 45.8 %
B
Secreted proteins
Color Key
25 30 35
Value
VBNC
Hypoxia
D6
D4
STAT
D4
Normoxia
D6
D8
C
Cellular proteins
Normoxia
D4
D8
STAT
D6
D4
Hypoxia
D6
D8
VBNC
PC2 : 13.2 %
PC1 : 61.3 %
D
Cellular proteins
Color Key
25 30 35
Value
VBNC
Hypoxia
D6
D4
STAT
D4
Normoxia
D6
D8

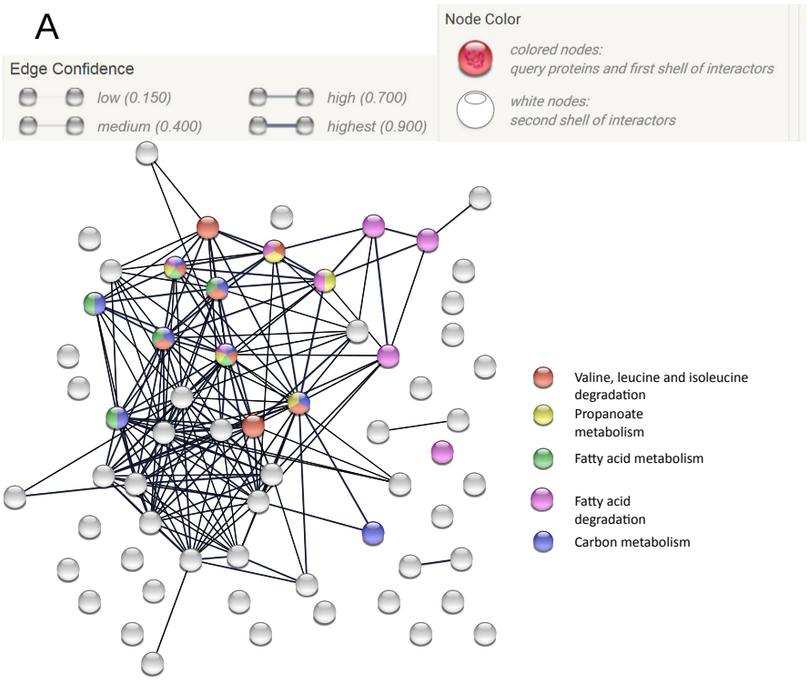
A
Edge Confidence
low (0.150)
medium (0.400)
high (0.700)
highest (0.900)
Node Color
colored nodes:
query proteins and first shell of interactors
white nodes:
second shell of interactors
Valine, leucine and isoleucine degradation
Propanoate metabolism
Fatty acid metabolism
Fatty acid degradation
Carbon metabolism

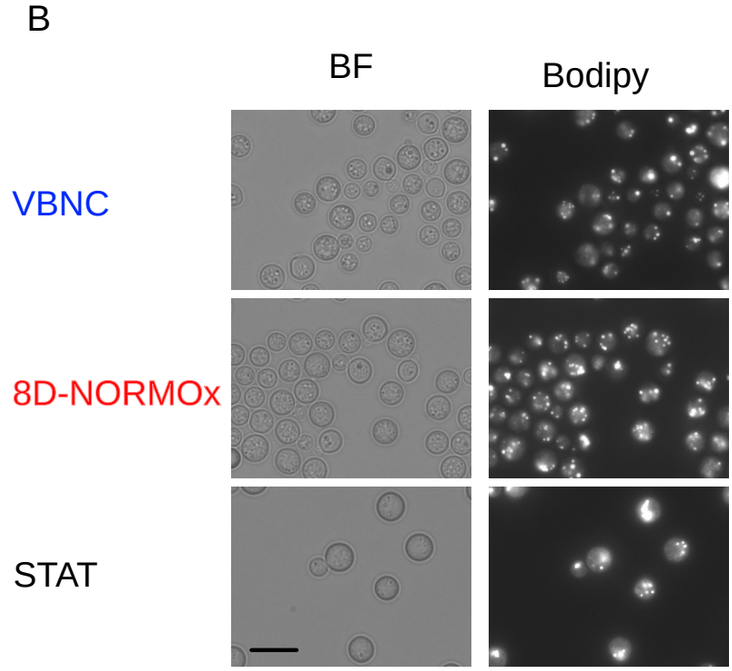
B
BF
Bodipy
VBNC
8D-NORMOx
STAT

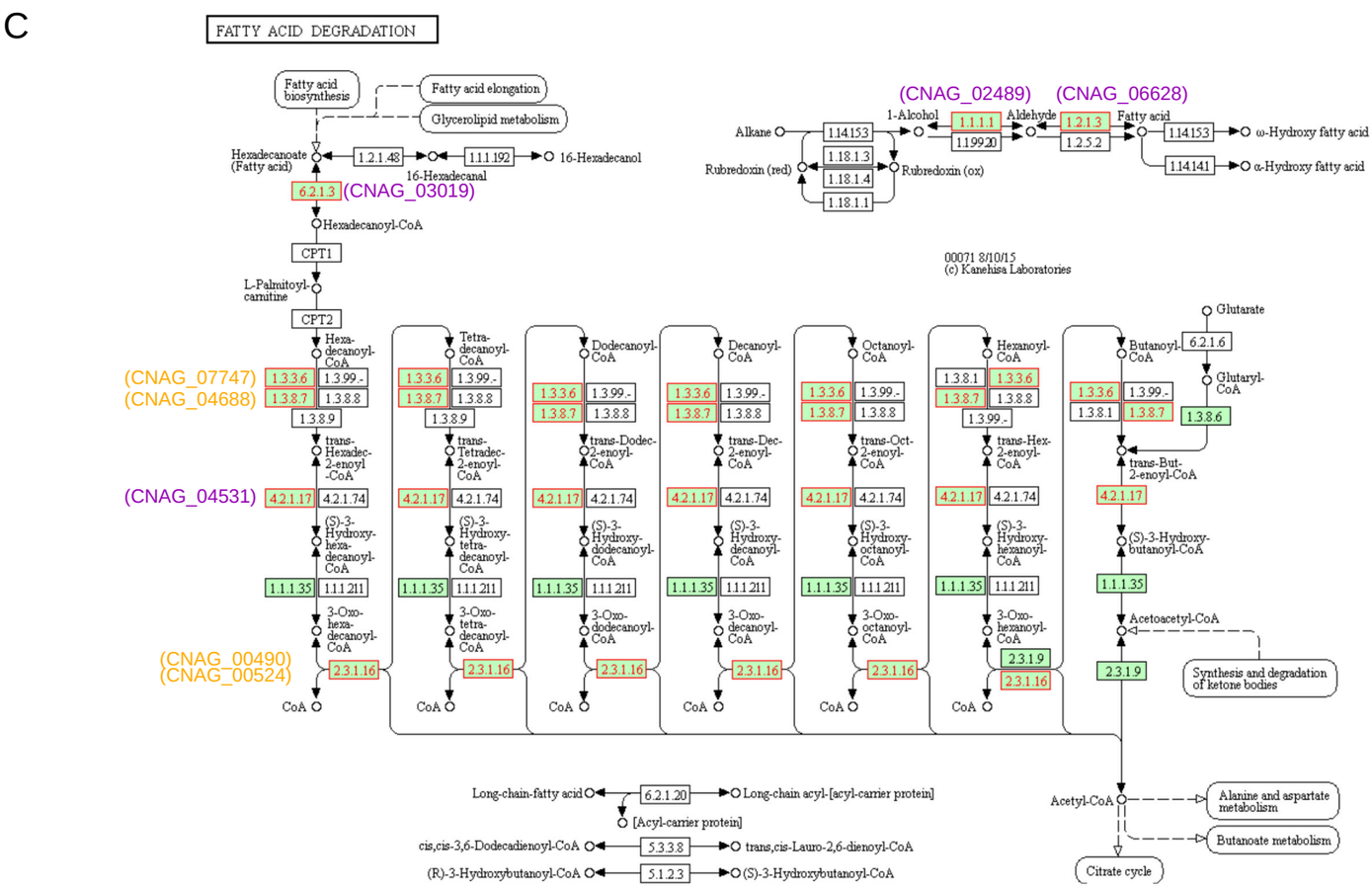
C
FATTY ACID DEGRADATION
Fatty acid biosynthesis
Fatty acid elongation
Glycerolipid metabolism
Hexadecanoate (Fatty acid)
1.2.1.48
1.1.1.192
16-Hexadecanol
16-Hexadecanal
6.2.1.3
(CNAG_03019)
Hexadecanoyl-CoA
CPT1
L-Palmitoyl-carnitine
CPT2
(CNAG_02489)
(CNAG_06628)
Alkane
1-Alcohol
Aldehyde
Fatty acid
Rubredoxin (red)
Rubredoxin (ox)
ω-Hydroxy fatty acid
α-Hydroxy fatty acid
00071 8/10/15
(c) Kanehisa Laboratories
(CNAG_07747)
(CNAG_04688)
(CNAG_04531)
(CNAG_00490)
(CNAG_00524)
Hexa-decanoyl-CoA
Tetra-decanoyl-CoA
Dodecanoyl-CoA
Decanoyl-CoA
Octanoyl-CoA
Hexanoyl-CoA
Butanoyl-CoA
Glutarate
Glutaryl-CoA
trans-Hexadec-2-enoyl-CoA
trans-Tetradec-2-enoyl-CoA
trans-Dodec-2-enoyl-CoA
trans-Dec-2-enoyl-CoA
trans-Oct-2-enoyl-CoA
trans-Hex-2-enoyl-CoA
trans-But-2-enoyl-CoA
(S)-3-Hydroxy-hexa-decanoyl-CoA
(S)-3-Hydroxy-tetra-decanoyl-CoA
(S)-3-Hydroxy-dodecanoyl-CoA
(S)-3-Hydroxy-decanoyl-CoA
(S)-3-Hydroxy-octanoyl-CoA
(S)-3-Hydroxy-hexanoyl-CoA
(S)-3-Hydroxy-butanoyl-CoA
3-Oxo-hexa-decanoyl-CoA
3-Oxo-tetra-decanoyl-CoA
3-Oxo-dodecanoyl-CoA
3-Oxo-decanoyl-CoA
3-Oxo-octanoyl-CoA
3-Oxo-hexanoyl-CoA
Acetoacetyl-CoA
Synthesis and degradation of ketone bodies
CoA
Long-chain-fatty acid
6.2.1.20
Long-chain acyl-[acyl-carrier protein]
[Acyl-carrier protein]
cis,cis-3,6-Dodecadienoyl-CoA
5.3.3.8
trans,cis-Lauro-2,6-dienoyl-CoA
(R)-3-Hydroxybutanoyl-CoA
5.1.2.3
(S)-3-Hydroxybutanoyl-CoA
Acetyl-CoA
Alanine and aspartate metabolism
Butanoate metabolism
Citrate cycle

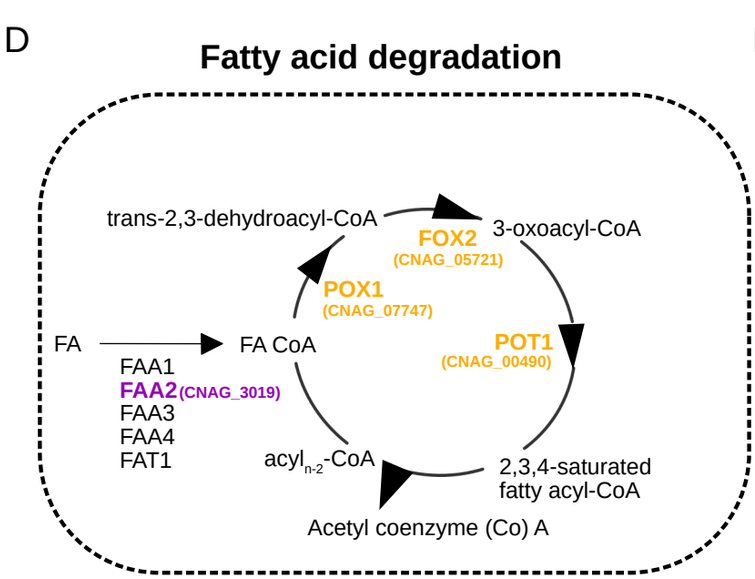
D
Fatty acid degradation
trans-2,3-dehydroacyl-CoA
FOX2
(CNAG_05721)
3-oxoacyl-CoA
POX1
(CNAG_07747)
FA
FA CoA
POT1
(CNAG_00490)
FAA1
FAA2 (CNAG_3019)
FAA3
FAA4
FAT1
acyl$_{n-2}$-CoA
2,3,4-saturated fatty acyl-CoA
Acetyl coenzyme (Co) A

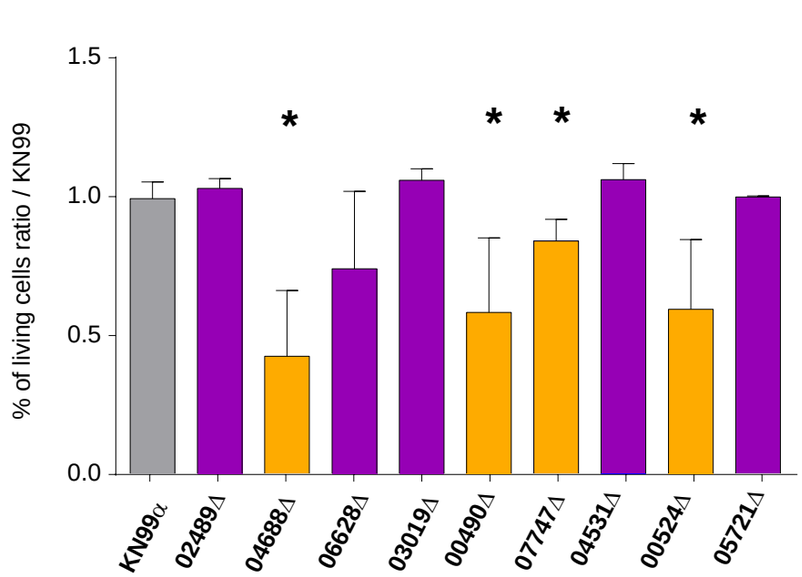
E
% of living cells ratio / KN99
1.5
1.0
0.5
0.0
*
*
*
*
KN99α
02489Δ
04688Δ
06628Δ
03019Δ
00490Δ
07747Δ
04531Δ
00524Δ
05721Δ

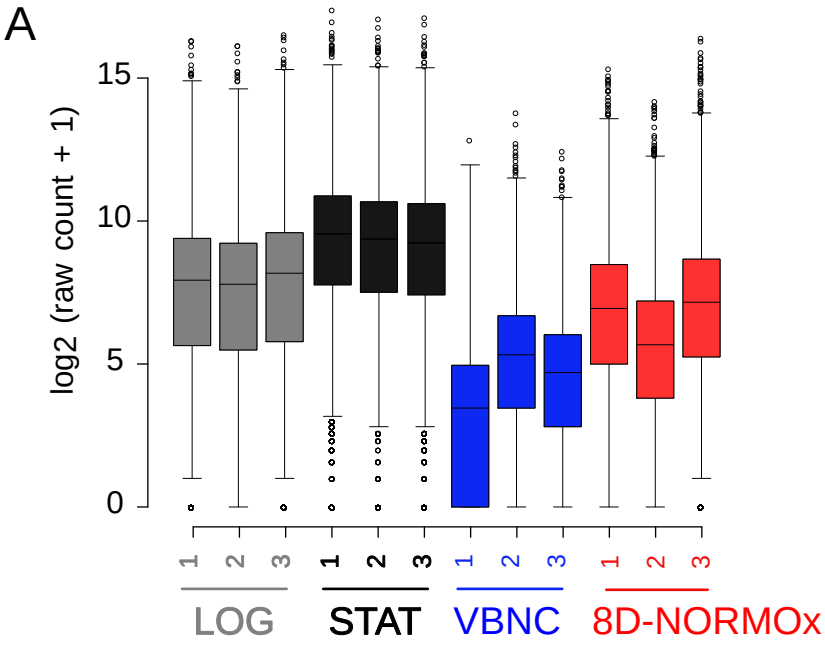
A
log2 (raw count + 1)
15
10
5
0
1 2 3 1 2 3 1 2 3 1 2 3
LOG
STAT
VBNC
8D-NORMOx

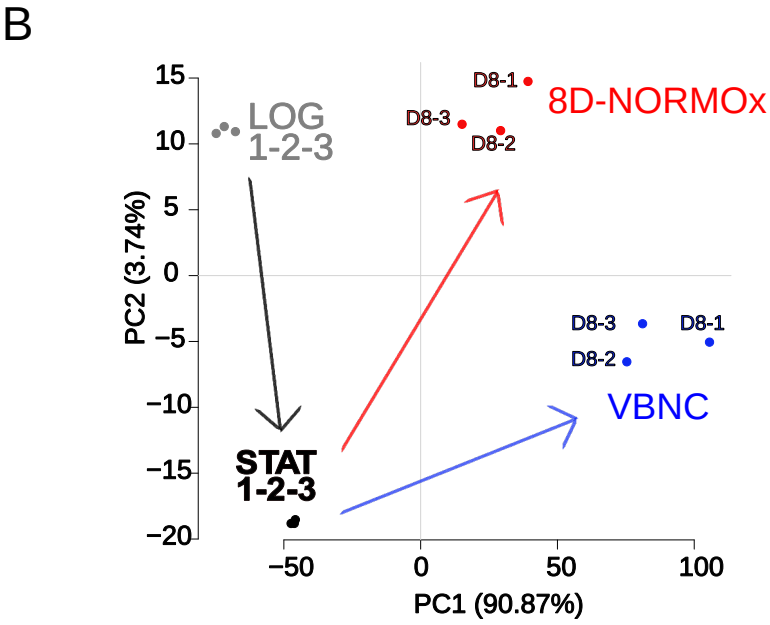
B
PC2 (3.74%)
PC1 (90.87%)
15
10
5
0
−5
−10
−15
−20
−50
0
50
100
LOG
1-2-3
STAT
1-2-3
D8-1
D8-3
D8-2
8D-NORMOx
D8-3
D8-1
D8-2
VBNC

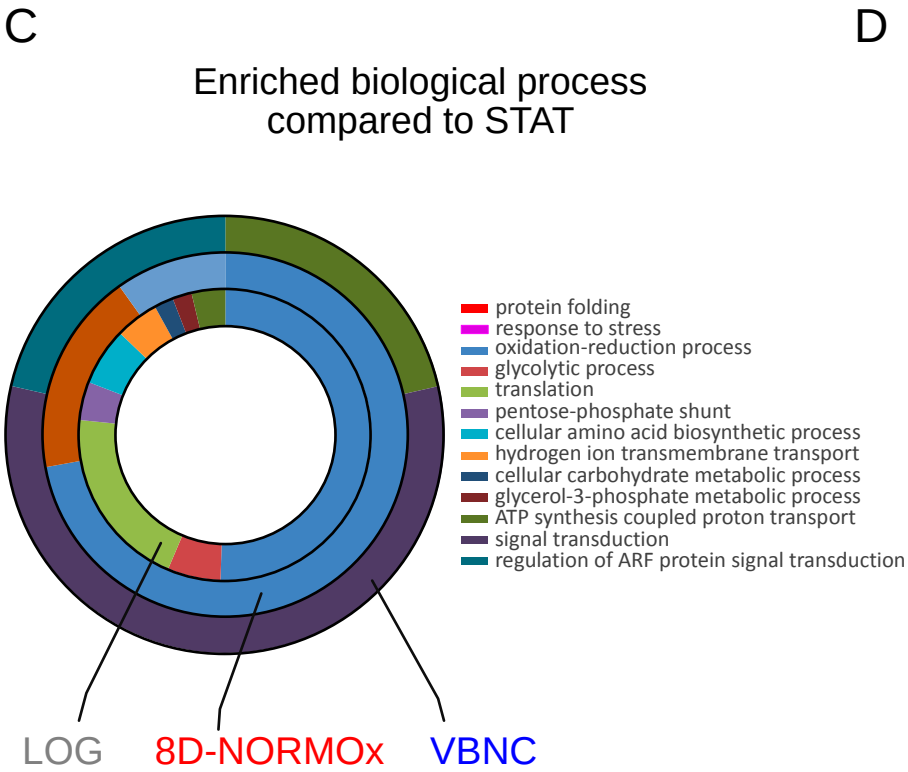
C
Enriched biological process
compared to STAT
protein folding
response to stress
oxidation-reduction process
glycolytic process
translation
pentose-phosphate shunt
cellular amino acid biosynthetic process
hydrogen ion transmembrane transport
cellular carbohydrate metabolic process
glycerol-3-phosphate metabolic process
ATP synthesis coupled proton transport
signal transduction
regulation of ARF protein signal transduction
LOG
8D-NORMOx
VBNC

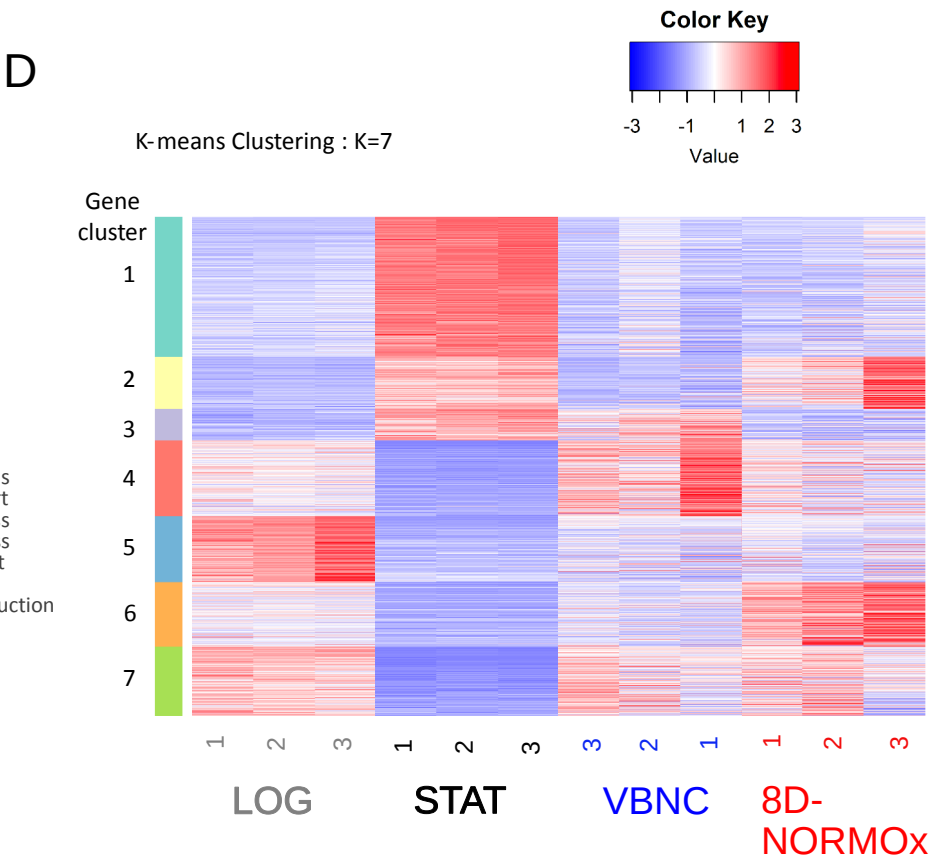
D
Color Key
-3
-1
1
2
3
Value
K-means Clustering : K=7
Gene
cluster
1
2
3
4
5
6
7
1 2 3 1 2 3 3 2 1 1 2 3
LOG
STAT
VBNC
8D-
NORMOx

Table 1 : Cell dilutions and latency related to the culture medium and their extrapolated equation

Cell dilutions	**Latency (min)**			
	YPD		MM	
	STAT	8D-HYPOx	STAT	8D-HYPOx
$3x10^5$	544 [409-732]	1764 [1605-1903]		
$3x10^4$	789 [641-958]	2030 [1902-2228]	585 [515-602]	2732 [2548-2903]
$3x10^3$	1037 [879-1223]	2356 [2264-2838]	1120 [1101-1154]	4124 [3741-4360]
$3x10^2$	1330 [1205-1501]	2680 [2381-3197]	2408 [2058-2502]	4668 [4353-5140]
$3x10^1$	1657 [1485-1801]	3557 [2924-3810]	3399 [3003-3618]	4483 [4354-5277]
3	2044 [1919-2241]		4127 [4093-4336]	
Equation (R^2)	Y=2127-296logX (0.90)	Y=3947-408logX (0.59)	Y=4632-941logX (0.97)	Y=6603-810logX (0.74)

Table 2: Metabolic pathways regulatd in hypoxia by STRING analysis

Metabolic pathways	Genes	Corrected *p* value (FDR 1%)
Fatty acid degradation	CNAG_00490, CNAG_00524, CNAG_03019, CNAG_02489, CNAG_06628, CNAG_07747, CNAG_04531, CNAG_04688	1,20E-09
Valine, leucine and isoleucine degradation	CNAG_00484, CNAG_00490, CNAG_00524, CNAG_03067, CNAG_06628, CNAG_04531, CNAG_04351, CNAG_04688	2,40E-08
Fatty acid metabolism	CNAG_00490, CNAG_00524, CNAG_03019, CNAG_07747, CNAG_04531, CNAG_04688	9,50E-07
Propanoate metabolism	CNAG_00797, CNAG_06628, CNAG_04531, CNAG_04351, CNAG_04688	4,00E-05
Carbon metabolism	CNAG_00797, CNAG_00826, CNAG_05653, CNAG_05303, CNAG_04531, CNAG_04351, CNAG_04217, CNAG_04688	4,00E-05
Biosynthesis of secondary metabolites	CNAG_00484, CNAG_00490, CNAG_00524, CNAG_00797, CNAG_03067, CNAG_02489, CNAG_06628, CNAG_04531, CNAG_04217, CNAG_04688, CNAG_06431	2,60E-04
Peroxisome	CNAG_00537, CNAG_03067, CNAG_03019, CNAG_06551, CNAG_07747	2,90E-04
Metabolic pathways	CNAG_00484, CNAG_00490, CNAG_00524, CNAG_00797, CNAG_00826, CNAG_03067, CNAG_03019, CNAG_01540, CNAG_02489, CNAG_06628, CNAG_07747, CNAG_05653, CNAG_05303, CNAG_04531, CNAG_04351, CNAG_04217, CNAG_04688	3,60E-04
beta-Alanine metabolism	CNAG_06628, CNAG_04531, CNAG_04351, CNAG_04688	4,50E-04
Microbial metabolism in diverse environments	CNAG_00490, CNAG_00797, CNAG_02489, CNAG_06628, CNAG_05653, CNAG_05303, CNAG_04531, CNAG_04217	4,70E-04
alpha-Linolenic acid metabolism	CNAG_00490, CNAG_07747	8,50E-04
Pyruvate metabolism	CNAG_00797, CNAG_06628, CNAG_05653, CNAG_04217	2,40E-03
Glycolysis / Gluconeogenesis	CNAG_00797, CNAG_02489, CNAG_06628, CNAG_04217	2,80E-03
Butanoate metabolism	CNAG_03067, CNAG_02045, CNAG_04531	7,20E-03
Fatty acid elongation	CNAG_00524, CNAG_04531	2,20E-02

Table 3: Transcriptomic pathways involved in the VBNC cluster 3 and genes the corresponding upregulated genes.

Source	ID	Name	Result gene list	Fold enrichment	Odds ratio	P-value	Benjamini Hochberg correction
GO	GO:0006468	protein phosphorylation	CNAG_00769,CNAG_01905,CNAG_02389,CNAG_02820,CNAG_03216,CNAG_03670,CNAG_04040,CNAG_04755,CNAG_05439,CNAG_06193,CNAG_06310,CNAG_06490,CNAG_06845,	3.59	3.84	1.3E-04	1.8E-03
GO	GO:0016310	phosphorylation	CNAG_00769,CNAG_01905,CNAG_02389,CNAG_02820,CNAG_03216,CNAG_03670,CNAG_04040,CNAG_04755,CNAG_05439,CNAG_06193,CNAG_06310,CNAG_06490,CNAG_06845,	2.9	3.08	8.7E-04	6.1E-03
GO	GO:0050789	regulation of biological process	CNAG_00332,CNAG_00547,CNAG_00818,CNAG_01258,CNAG_01533,CNAG_01611,CNAG_01841,CNAG_03212,CNAG_03763,CNAG_03902,CNAG_04036,CNAG_04243,CNAG_04496,CNAG_05535,CNAG_05695,CNAG_05861,CNAG_06188,CNAG_06531,CNAG_06606,CNAG_06691,CNAG_06814,CNAG_07015,CNAG_07320,CNAG_07470,CNAG_07506,CNAG_07921,	1.79	1.95	3.2E-03	6.4E-03
GO	GO:0023051	regulation of signaling	CNAG_00547,CNAG_01258,CNAG_01611,CNAG_03763,CNAG_04243,CNAG_07015,	4.54	4.7	3.3E-03	6.4E-03
GO	GO:0048583	regulation of response to stimulus	CNAG_00547,CNAG_01258,CNAG_01611,CNAG_03763,CNAG_04243,CNAG_07015,	4.54	4.7	3.3E-03	6.4E-03
GO	GO:0010646	regulation of cell communication	CNAG_00547,CNAG_01258,CNAG_01611,CNAG_03763,CNAG_04243,CNAG_07015,	4.54	4.7	3.3E-03	6.4E-03
GO	GO:0009966	regulation of signal transduction	CNAG_00547,CNAG_01258,CNAG_01611,CNAG_03763,CNAG_04243,CNAG_07015,	4.54	4.7	3.3E-03	6.4E-03
GO	GO:0065007	biological regulation	CNAG_00332,CNAG_00547,CNAG_00818,CNAG_01258,CNAG_01533,CNAG_01611,CNAG_01841,CNAG_03212,CNAG_03763,CNAG_03902,CNAG_04036,CNAG_04243,CNAG_04496,CNAG_05535,CNAG_05695,CNAG_05861,CNAG_06188,CNAG_06531,CNAG_06606,CNAG_06691,CNAG_06814,CNAG_07015,CNAG_07320,CNAG_07470,CNAG_07506,CNAG_07921,	1.74	1.91	4.3E-03	6.4E-03

GO	GO:0036211	protein modification process	CNAG_00498,CNAG_00769,CNAG_01385,CNAG_01905,CNAG_02389,CNAG_02820,CNAG_03216,CNAG_03670,CNAG_04040,CNAG_04755,CNAG_05439,CNAG_06193,CNAG_06310,CNAG_06490,CNAG_06845,	2.2	2.33	4.6E-03	6.4E-03
GO	GO:0006464	cellular protein modification process	CNAG_00498,CNAG_00769,CNAG_01385,CNAG_01905,CNAG_02389,CNAG_02820,CNAG_03216,CNAG_03670,CNAG_04040,CNAG_04755,CNAG_05439,CNAG_06193,CNAG_06310,CNAG_06490,CNAG_06845,	2.2	2.33	4.6E-03	6.4E-03
GO	GO:0035023	regulation of Rho protein signal transduction	CNAG_00547,CNAG_01258,CNAG_04243,CNAG_07015,	6.63	6.78	5.2E-03	6.6E-03
GO	GO:0050794	regulation of cellular process	CNAG_00332,CNAG_00547,CNAG_01258,CNAG_01533,CNAG_01611,CNAG_01841,CNAG_03212,CNAG_03763,CNAG_03902,CNAG_04036,CNAG_04243,CNAG_05535,CNAG_05695,CNAG_05861,CNAG_06188,CNAG_06531,CNAG_06606,CNAG_06691,CNAG_06814,CNAG_07015,CNAG_07320,CNAG_07470,CNAG_07506,CNAG_07921,	1.75	1.89	6.0E-03	7.0E-03
GO	GO:0051056	regulation of small GTPase mediated signal transduction	CNAG_00547,CNAG_01258,CNAG_03763,CNAG_04243,CNAG_07015,	4.57	4.7	7.0E-03	7.0E-03
GO	GO:1902531	regulation of intracellular signal transduction	CNAG_00547,CNAG_01258,CNAG_03763,CNAG_04243,CNAG_07015,	4.57	4.7	7.0E-03	7.0E-03
KEGG	ec00900__PK__KEGG	Terpenoid backbone biosynthesis	CNAG_02662,CNAG_03216,CNAG_05601,CNAG_06534,CNAG_07377,	4.74	5.26	4.7E-03	